

# Sourcing Dark Matter and Dark Energy from $\alpha$ -attractors

Swagat S. Mishra,<sup>a</sup> Varun Sahni<sup>a</sup> and Yuri Shtanov<sup>b,c</sup>

<sup>a</sup>Inter-University Centre for Astronomy and Astrophysics, Post Bag 4, Ganeshkhind, Pune 411 007, India

<sup>b</sup>Bogolyubov Institute for Theoretical Physics, Kiev 03680, Ukraine

<sup>c</sup>Department of Physics, Taras Shevchenko Kiev National University, Kiev, Ukraine

E-mail: [swagat@iucaa.in](mailto:swagat@iucaa.in), [varun@iucaa.in](mailto:varun@iucaa.in), [shtanov@bitp.kiev.ua](mailto:shtanov@bitp.kiev.ua)

**Abstract.** In [1], Kallosh and Linde drew attention to a new family of superconformal inflationary potentials, subsequently called  $\alpha$ -attractors [2]. The  $\alpha$ -attractor family can interpolate between a large class of inflationary models. It also has an important theoretical underpinning within the framework of supergravity. We demonstrate that the  $\alpha$ -attractors have an even wider appeal since they may describe dark matter and perhaps even dark energy. The dark matter associated with the  $\alpha$ -attractors, which we call  $\alpha$ -dark matter ( $\alpha$ DM), shares many of the attractive features of *fuzzy* dark matter, with  $V(\varphi) = \frac{1}{2}m^2\varphi^2$ , while having none of its drawbacks. Like fuzzy dark matter,  $\alpha$ DM can have a large Jeans length which could resolve the cusp–core and substructure problems faced by standard cold dark matter.  $\alpha$ DM also has an appealing tracker property which enables it to converge to the late-time dark matter asymptote,  $\langle w \rangle \simeq 0$ , from a wide range of initial conditions. It thus avoids the enormous fine-tuning problems faced by the  $m^2\varphi^2$  potential in describing dark matter.

**Keywords:** dark matter theory, dark energy theory

---

## Contents

<b>1</b>	<b>Introduction</b>	<b>1</b>
<b>2</b>	<b>Conformal inflation</b>	<b>2</b>
<b>3</b>	<b>Conformal dark matter</b>	<b>3</b>
<b>4</b>	<b>Dark Matter</b>	<b>5</b>
4.1	Dark Matter from the potential $\frac{1}{2}m^2\varphi^2$	5
4.2	Dark Matter from the <i>E-Model</i>	10
4.2.1	Evolution along the tracker wing	10
4.2.2	Evolution along the flat wing	13
4.3	Dark Matter from the Tracker Model	18
4.4	Dark Matter from the T-Model	20
4.5	Gravitational Instability	21
<b>5</b>	<b>Dark Energy</b>	<b>26</b>
5.1	Dark Energy from the potential $V \propto  \varphi ^{2n}$	26
5.2	Dark Energy from the asymmetric <i>E-Model</i>	28
<b>6</b>	<b>Discussion</b>	<b>31</b>
<b>A</b>	<b>Linear perturbations and instability</b>	<b>33</b>
<b>B</b>	<b>Parametric resonance to second order</b>	<b>35</b>
<b>C</b>	<b>Relationship between the mass of the scalar field and its initial value</b>	<b>39</b>

---

## 1 Introduction

Dark matter (DM) and dark energy (DE) are two of the most enigmatic observables in current cosmology. While dark matter is assumed to be pressureless, dark energy is believed to have large negative pressure which accelerates the present universe. Nothing significantly more is known about the nature of either dark matter or dark energy. It is accepted that dark matter must cluster, in order to account for the missing-mass problem associated with individual galaxies and with galaxy clusters. Furthermore, there are strong reasons to believe that dark matter must have already been in place by redshifts of  $z \gtrsim 10^4$ . This is indicated by primordial fluctuations in the cosmic microwave background (CMB), whose small amplitude ( $\Delta T/T \sim 10^{-5}$ ) is suggestive of an equally small amplitude of primordial density fluctuations at  $z \gtrsim 10^3$ . Such small fluctuations would have had difficulty in growing to the much larger values today,  $\delta\rho/\rho > \mathcal{O}(1)$ , in a universe consisting solely of baryons [3, 4].

The origin of dark energy could, on the other hand, be much more recent, since there is observational evidence to suggest that the universe commenced accelerating at  $z \lesssim \text{few}$ .

Theoretical models of dark matter usually subscribe to the view that it is made up of hitherto undetected elementary particles called WIMPs (weakly interacting massive particles). However, despite several decades of systematic searches by elaborate experiments, a

firm consensus on the existence of WIMPs has eluded researchers. Our understanding of dark energy faces an even greater dilemma since its basic properties, such as its pressure and density, have only been indirectly deduced via cosmological observations of the expansion history,  $H(z)$ , or the luminosity distance,  $D_L(z)$ . Consequently, it has even been suggested that both DM & DE may owe their origin to a modification of the laws of gravity on large scales [5, 6].

In this paper, we move past the dominant paradigm of particle-like WIMP dark matter and examine the alternative possibility that DM could have the structure of a scalar field. Ever since the advent of Inflation, scalar field models have played an increasingly prominent role in our understanding of the very early universe. Scalar-field models have also been advocated to describe dark energy [6]. Recently, Kallosh and Linde [1] have discussed a new class of scalar-field models, called  $\alpha$ -attractors [2], which have an attractive feature of describing an entire family of inflationary models within a common theoretical setting. In this paper, we show how the  $\alpha$ -attractors may have an even wider appeal, since they can describe dark matter, and perhaps even dark energy.

Our paper is structured as follows: section 2 discusses the  $\alpha$ -attractor Lagrangian in the context of conformal inflation, while section 3 discusses the  $\alpha$ -attractor Lagrangian in the context of dark matter and dark energy. Section 4 explores the role of  $\alpha$ -attractors as dark matter and includes a comprehensive discussion of gravitational instability. Section 5 discusses  $\alpha$ -attractors in the context of dark energy. A summary of our results is presented in section 6, in which we also discuss the possibility that the inflaton could play the role of dark matter at late times, after preheating.

## 2 Conformal inflation

In [1], Kallosh & Linde drew attention to an interesting new family of potentials which could give rise to successful inflation. The starting point of this discovery was the observation that the action with the Lagrangian

$$\mathcal{L} = \sqrt{-g} \left[ \frac{1}{2} \partial_\mu \chi \partial^\mu \chi + \frac{\chi^2}{12} R(g) - \frac{1}{2} \partial_\mu \phi \partial^\mu \phi - \frac{\phi^2}{12} R(g) - \frac{\tilde{\lambda}}{4} (\phi^2 - \chi^2)^2 \right], \quad (2.1)$$

where  $\chi$  and  $\phi$  are scalar fields, and  $\tilde{\lambda}$  is a dimensionless constant, is invariant under the  $O(1,1)$  group of transformations in the  $(\chi, \phi)$  space and also under the group of local conformal transformations. When the local conformal gauge is fixed to

$$\chi^2 - \phi^2 = 6m_p^2, \quad (2.2)$$

this Lagrangian can be parameterized by

$$\chi = \sqrt{6}m_p \cosh \frac{\varphi}{\sqrt{6}m_p}, \quad \phi = \sqrt{6}m_p \sinh \frac{\varphi}{\sqrt{6}m_p}, \quad (2.3)$$

and reduces to

$$L = \sqrt{-g} \left[ \frac{m_p^2}{2} R - \frac{1}{2} \partial_\mu \varphi \partial^\mu \varphi - 9\tilde{\lambda}m_p^4 \right], \quad (2.4)$$

describing Einstein's gravity with the reduced Planck mass  $m_p = 1/\sqrt{8\pi G} \approx 2.4 \times 10^{18}$  GeV and cosmological constant  $\Lambda = 9\tilde{\lambda}m_p^2$ . A conformally invariant generalization of (2.1)  $\tilde{\lambda} \rightarrow$

$F(\phi/\chi)/9$ , with an arbitrary function  $F$  that deforms the  $O(1,1)$  symmetry, results in the standard Lagrangian

$$\mathcal{L} = \sqrt{-g} \left[ \frac{m_p^2}{2} R - \frac{1}{2} \partial_\mu \varphi \partial^\mu \varphi - V(\varphi) \right] \quad (2.5)$$

with a scalar-field potential

$$V(\varphi) = m_p^4 F \left( \tanh \frac{\varphi}{\sqrt{6} m_p} \right). \quad (2.6)$$

In [1], various canonical potentials  $V(\varphi)$  were investigated in the context of inflation. In [2], a family of potentials called  $\alpha$ -attractors were considered following the prescription  $V(\varphi) \rightarrow V(\varphi/\sqrt{\alpha})$  starting from canonical potentials  $V(\varphi)$  in (2.6). The  $\alpha$ -attractors are able to parameterize a wide variety of inflationary settings including chaotic inflation and the Starobinsky model. (The parameter  $\alpha$  was shown to be related to the curvature of the superconformal Kähler metric in [2].)

### 3 Conformal dark matter

In this paper, we would like to demonstrate that the theory of the previous section can also describe dark matter and perhaps even dark energy. To this end, we first incorporate the scalar-field Lagrangian

$$\mathcal{L} = \sqrt{-g} \left[ \frac{1}{2} \partial_\mu \chi \partial^\mu \chi + \frac{\chi^2}{12} R(g) - \frac{1}{2} \partial_\mu \phi \partial^\mu \phi - \frac{\phi^2}{12} R(g) - \frac{F(\phi/\chi)}{36 m_p^4} (\phi^2 - \chi^2)^2 \right] \quad (3.1)$$

into the Standard Model (SM) of electroweak interactions respecting the local conformal invariance. Since the only sector in the SM that breaks conformal invariance is the kinetic and potential terms of the Higgs field  $h$ , we modify the relevant parts in the minimal possible way:

$$\mathcal{L}_h = -\sqrt{-g} \left( \frac{1}{2} \partial_\mu h \partial^\mu h + \frac{h^2}{12} R + \frac{\lambda_h}{4} \left[ h^2 - \frac{v^2}{6 m_p^2} (\chi^2 - \phi^2) \right]^2 \right), \quad (3.2)$$

where  $v \approx 246$  GeV is the Higgs-field vacuum expectation value, and  $\lambda_h$  is its self-coupling constant. After fixing the conformal gauge as in (2.2), we obtain a theory with the Lagrangian

$$\mathcal{L} = \sqrt{-g} \left[ \frac{m_p^2 - h^2/6}{2} R - \frac{1}{2} \partial_\mu \varphi \partial^\mu \varphi - V(\varphi) \right] + \mathcal{L}_{\text{SM}}, \quad (3.3)$$

where  $V(\varphi)$  is given by (2.6), and  $\mathcal{L}_{\text{SM}}$  is the canonical Lagrangian of the SM fields and interactions. The term  $h^2 R/12$  which enters (3.3) with negative sign, and which was required to ensure the conformal invariance of the original action (3.2), will produce a small negative contribution to the gravitational action, which will result in the eventual gravitational coupling equal to  $m_p^2 - v^2/6 \approx m_p^2$ .

In the above model, the scalar field  $\varphi$  interacts with the rest of matter only via gravity. Thus, the dark matter described by such a scalar would either have coexisted with the

inflaton, or it would have to be produced, together with its perturbations, by a quantum mechanism towards the end of the inflationary epoch.<sup>1</sup>

Our primary focus in this paper will be on the following potentials belonging to the  $\alpha$ -attractor family, following the prescription  $V(\varphi) \rightarrow V(\varphi/\sqrt{\alpha})$  in (2.6):

1. The asymmetric *E-Model* [2]

$$V(\varphi) = V_0 \left( 1 - e^{-\sqrt{\frac{2}{3\alpha}} \frac{\varphi}{m_p}} \right)^{2n} \equiv 2V_0 \left[ \frac{\tanh \frac{\varphi}{\sqrt{6\alpha}m_p}}{1 + \tanh \frac{\varphi}{\sqrt{6\alpha}m_p}} \right]^{2n}. \quad (3.4)$$

which reduces to the potential associated with Starobinsky inflation [7] when  $\alpha = 1$ ,  $n = 1$ .

2. The tracker-potential<sup>2</sup> [8]

$$V(\varphi) = V_0 \sinh^{2n} \sqrt{\frac{2}{3\alpha}} \frac{\varphi}{m_p} \equiv V_0 \left[ \frac{\tanh^2 \sqrt{\frac{2}{3\alpha}} \frac{\varphi}{m_p}}{1 - \tanh^2 \sqrt{\frac{2}{3\alpha}} \frac{\varphi}{m_p}} \right]^n. \quad (3.5)$$

3. The *T-Model* potential [1]

$$V(\varphi) = V_0 \tanh^{2n} \frac{\varphi}{\sqrt{6\alpha}m_p}. \quad (3.6)$$

An important feature of all of the above potentials is that they have the same asymptotic form  $V(\varphi) \sim V_0 \left( \frac{\varphi}{\sqrt{6\alpha}m_p} \right)^{2n}$  for  $\frac{\varphi}{\sqrt{6\alpha}} \ll m_p$ . It is well known that a scalar field oscillating about the minimum of such a potential will have the time-averaged equation of state (EOS) [9]

$$\langle w \rangle = \left\langle \frac{p}{\rho} \right\rangle = \frac{n-1}{n+1}. \quad (3.7)$$

Consequently, for  $n = 1$ , the scalar field will be pressureless, just like dark matter. For  $n < 1/2$ , on the other hand, the EOS  $\langle w \rangle < -1/3$  violates the strong energy condition. Such a field could therefore play the role of dark energy by causing the universe to accelerate [8].

---

<sup>1</sup>If we were to construct models of inflation, as done in [1, 2], we would have to provide for interaction of the inflaton field  $\varphi$  with matter fields, in order that the universe could be reheated. This could be done, for instance, by replacing the constant  $\lambda_h$  in (3.2) by another conformally invariant function  $G(\phi/\chi)$  such that, at the minimum of the potential  $V(\varphi)$ , the function  $W(\varphi) \equiv G\left(\tanh \frac{\varphi}{\sqrt{6\alpha}m_p}\right)$  acquires the value  $\lambda_h$ . For the present case, where the scalar field  $\varphi$  represents dark matter, such a coupling seems to be unnecessary, and perhaps not even desirable.

<sup>2</sup>Note that the tracker potential described by (3.5) is not a member of the inflationary  $\alpha$ -attractor family, which were defined to have a restricted dependence on  $\tanh\left(\frac{\varphi}{\sqrt{6\alpha}m_p}\right)$  in order to possess a plateau. However, (3.5) turns out to be very useful as a model of DM (and DE).

## 4 Dark Matter

The observation that a coherently oscillating scalar field could play the role of dark matter is not new. One of the earliest DM candidates that drew on this possibility was the axion [10]. Indeed, after the global  $U(1)$  Peccei–Quinn symmetry is spontaneously broken, the pseudo-Goldstone boson of the broken symmetry, the axion, begins to oscillate under the influence of the potential

$$V(\varphi) = V_0 \left[ 1 - \cos \left( \frac{\varphi}{f} \right) \right]. \quad (4.1)$$

In the neighbourhood of the minimum of this potential, we have  $V(\varphi) \simeq \frac{1}{2}m_a^2\varphi^2$  where  $m_a^2 = V_0/f^2$  is the axion mass and  $f$  is the symmetry breaking scale. For the QCD axion, the symmetry breaking scale is experimentally bounded by  $f \geq 10^9$  GeV. Other phenomenological models of scalar-field dark matter have been explored in [8, 11–17].

An important aspect of scalar-field dark matter (SFDM) is that if the scalar field mass is small, then the Jeans length  $\lambda_J$  associated with gravitational clustering can be very large. For the canonical massive scalar field potential

$$V(\varphi) = \frac{1}{2}m^2\varphi^2, \quad (4.2)$$

one finds [11, 15]

$$\lambda_J = \pi^{3/4}(G\rho)^{-1/4}m^{-1/2}. \quad (4.3)$$

An oscillating scalar field with a mass of  $10^{-22}$  eV would therefore have a Jeans length of a few kiloparsec. Such a large Jeans length would inhibit gravitational clustering on small scales thereby helping to resolve the cusp–core dilemma faced by standard cold dark matter (CDM) in the context of dwarf spheroidal galaxies [8, 15, 18]. A macroscopically large Jeans length might also ameliorate the substructure problem in CDM. (Warm dark matter [19] and non-canonical scalar fields [20] provide another means of resolving these issues.) It is of interest to note that oscillations in the gravitational potential associated with SFDM can induce oscillations in the photon arrival time from millisecond pulsars. This effect may be detectable by future experiments such as the Square Kilometer Array (SKA) pulsar timing array [21] and laser interferometric gravitational wave detectors [22]. Finally, it is interesting to note that ultra-light scalar fields (pseudo Nambu–Goldstone bosons) arise naturally in string theory via the breaking of exact shift symmetry [18].

Several of these issues have been addressed in considerable detail in [18, 23, 24], therefore we do not delve any deeper into them in this paper. Instead, our focus will be on the class of initial conditions which can give rise to successful models of dark matter in the context of the  $\alpha$ -attractors. We shall commence our study with the canonical scalar-field potential  $V = \frac{1}{2}m^2\varphi^2$  and then move on to discuss the  $\alpha$ -attractor family of potentials (3.4), (3.5) & (3.6).

### 4.1 Dark Matter from the potential $\frac{1}{2}m^2\varphi^2$

The canonical potential for a scalar field describing dark matter is given by [11, 15]

$$V = \frac{1}{2}m^2\varphi^2. \quad (4.4)$$

For small values,  $\varphi \ll m_p$ , the scalar field oscillates about the minimum of its potential at  $\varphi = 0$ . As discussed earlier, the averaged equation of state during oscillations is  $\langle w_\varphi \rangle \simeq 0$  which allows the scalar field to behave like dark matter.

In order to gain a deeper appreciation of this dark-matter model, we must first turn to the radiative epoch, prior to the period when oscillations in  $\varphi$  commence.<sup>3</sup> It is believed that the density of radiation, soon after preheating, greatly exceeded the density of all other forms of matter in the universe. Consequently, the expansion history at this stage can be described by the equation

$$H^2 = \frac{8\pi G}{3} (\rho_r + \rho_\varphi + \rho_b + \dots) \simeq \frac{8\pi G}{3} \rho_r, \quad (4.5)$$

where

$$\rho_\varphi = \frac{1}{2} \dot{\varphi}^2 + V(\varphi), \quad p_\varphi = \frac{1}{2} \dot{\varphi}^2 - V(\varphi), \quad (4.6)$$

and the scalar field equation of motion is

$$\ddot{\varphi} + 3H\dot{\varphi} + V'(\varphi) = 0. \quad (4.7)$$

Since Hubble expansion is dominated by the radiation density, the scalar field experiences enormous damping as it attempts to roll down its potential (4.4). In the kinetic-dominated regime  $\dot{\varphi}^2 \gg V(\varphi)$ , the irrelevance of  $V'$  relative to the first two terms on the LHS of (4.7) ensures that the kinetic energy decreases rapidly, as  $\dot{\varphi}^2 \propto a^{-6}$ . This regime is then followed by slow-roll, during which the first term in (4.7) can be neglected. Consequently, in a very short span of time, the scalar field density comes to be dominated by the potential term leading to  $\rho_\varphi \simeq V(\varphi)$ . Clearly, since  $\varphi$  soon virtually stops evolving,  $V(\varphi)$  begins to play the role of a cosmological constant deep in the radiative stage. Figure 1 illustrates this fact.

---

<sup>3</sup>In particle-physics models of dark matter, dark matter appeared on the cosmological scene soon after post-inflationary preheating, together with radiation and other particles constituting the present universe. (Some of the particles present after reheating might have decayed away leaving behind only a secondary relic.) In the field-theoretic models of dark matter, such as the one under consideration in this paper, it is conceivable that the dark-matter field could have coexisted with the Inflaton as a spectator field, in which case it would generate a spectrum of isocurvature perturbations [25].

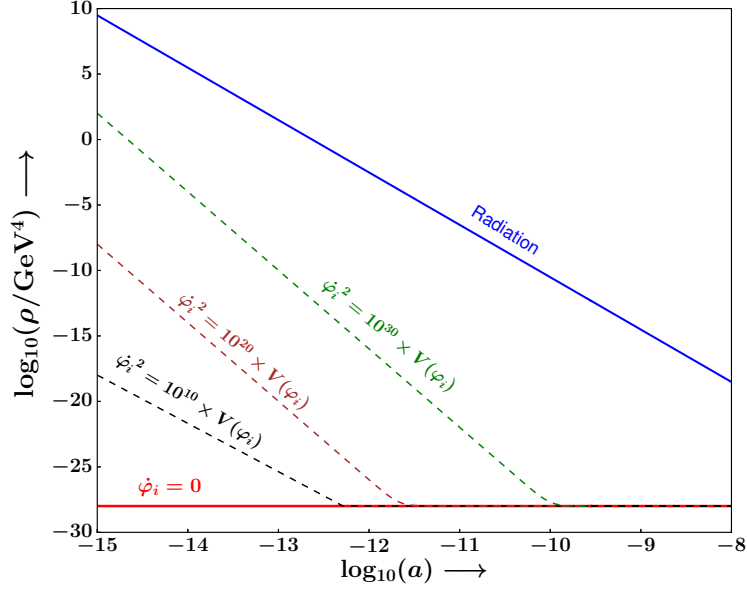


**Figure 1:** This figure demonstrates that, for  $V(\varphi) = \frac{1}{2}m^2\varphi^2$ , the scalar field velocity  $\dot{\varphi}$  rapidly decays in a radiation-dominated universe. Starting at  $a = 10^{-15}$  and fixing the initial field value to  $\varphi_i \simeq 0.06 m_p$ , we show that initially large kinetic terms rapidly get diluted, becoming irrelevant within a few  $N = \log_{10} a$  values. The black, brown and green dashed curves show the scalar-field energy density for fixed  $\varphi_i$ , and (lower to higher) initial kinetic energy values. One notes that all three curves converge towards the solid red line corresponding to  $\dot{\varphi}_i = 0$  by  $a \sim 10^{-10}$ . Consequently, the scalar field starts behaving like cosmological constant by  $z \sim 10^{10}$ . (For clarity of presentation, we do not show the baryon and dark energy density.)

Figure 1 illustrates that starting from a redshift  $z = 10^{15}$ , kinetic energy terms corresponding to different initial velocities  $\dot{\varphi}_i$  rapidly get damped, with the result that the scalar field begins to behave like cosmological constant by  $z \simeq 10^{10}$ . This is the redshift at which we set down initial conditions in our subsequent analysis.

The tendency of  $\rho_\varphi$  to behave like a cosmological constant deep within the radiative regime enormously influences the kind of initial conditions that need to be imposed on the scalar field in order that the model universe resemble ours (i.e., with  $\Omega_{0,\text{DE}} \simeq \frac{2}{3}$ ,  $\Omega_{0m} \simeq \frac{1}{3}$ ,  $\Omega_{0b} \simeq 0.04$ , and  $\Omega_{0r} \simeq 10^{-4}$ ). Figure 2 illustrates the enormous degree of fine-tuning associated with the initial density of the scalar field.



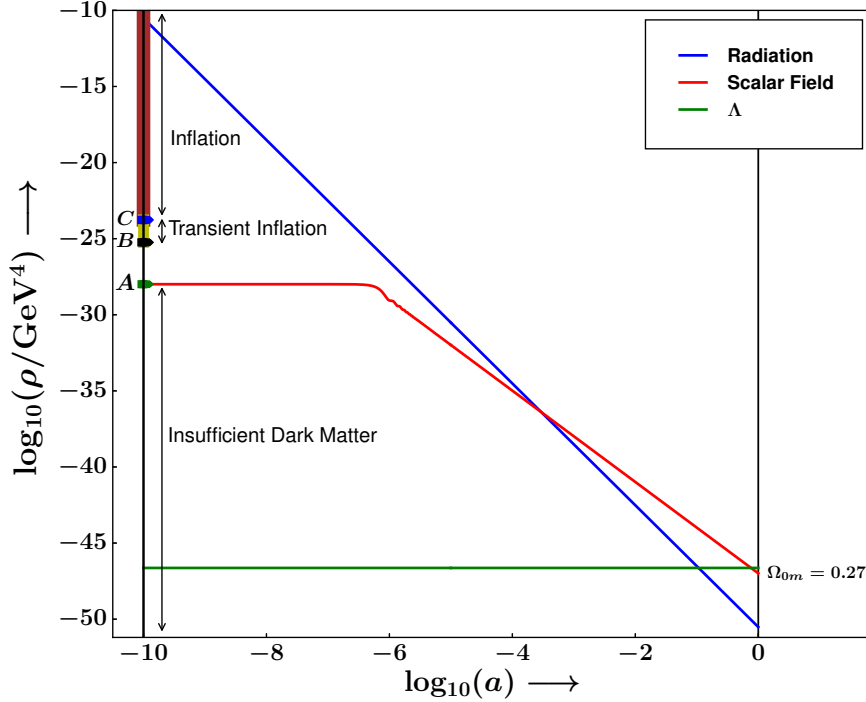


**Figure 2:** This figure describes the fine tuning associated with the initial scalar field density. Commencing our integration at  $a = 10^{-10}$  ( $z \simeq 10^{10}$ ), we find that the scalar-field energy density remains frozen to its initial value all the way until  $z \sim 10^6$ . The rapid decline in the radiation density from  $z = 10^{10}$  to  $z \sim 10^6$  reduces the damping on  $\varphi$  and releases the scalar field from its frozen value. Thereafter the scalar field begins to oscillate and behave like dark matter with  $\rho_\varphi \propto a^{-3}$ . The initial scalar-field value which results in  $\Omega_{0m} \simeq 0.27$  is shown by the green point A. The brown color band (commencing upwards from C) indicates the range of initial energy-density values which drive the universe into an inflating (accelerating) phase that lasts until the present epoch. The narrow green band with  $\rho_i \in (\rho_B, \rho_C)$  corresponds to a universe which experiences transient acceleration. Initial values of  $\rho_i < \rho_A$  result in an insufficient amount of dark matter at the present epoch ( $\Omega_{0m} < 0.27$ ) whereas  $\rho_A < \rho_i < \rho_B$  lead to too much dark matter. One, therefore, finds that, for a given value of  $m$  (in this case,  $10^{-22}$  eV), only a very narrow range of initial values of  $\varphi$  near point A can lead to a current value of  $\Omega_{0m}$  satisfying observational constraints. Namely,  $0.057 m_p \leq \varphi_i \leq 0.062 m_p$  results in  $\Omega_{0m} = 0.27 \pm 0.03$ . (For clarity of presentation, we do not show the baryon density.)

In constructing figure 2, we chose  $m = 10^{-22}$  eV. This ensures that the scalar field starts oscillating at  $z \sim 2.8 \times 10^6$ , after which it begins to behave like dark matter. For  $z > 10^6$ , the scalar field behaves like a cosmological constant. As remarked earlier, scalar-field dark matter with  $m \sim 10^{-22}$  eV would cluster on scales greater than a kiloparsec [15]. Three values of the initial scalar-field energy density,  $\rho_i$ , are of relevance for the present discussion. (i)  $\rho_i = \rho_A$ . This value of the initial energy density leads to a universe just like ours; in other words, if  $\rho_i = \rho_A$  then  $\Omega_{0m} \simeq 0.27$ . For  $m = 10^{-22}$  eV, one finds  $\rho_A = 1.02 \times 10^{-28}$  GeV<sup>4</sup>. Smaller initial values result in an insufficient amount of dark matter at the present epoch, i.e.  $\rho_i < \rho_A \Rightarrow \Omega_{0m} < 0.27$ .

(ii)  $\rho_i \in (\rho_B, \rho_C)$ . Initial values  $\rho_i \geq \rho_B$  lead to an accelerating (inflationary) phase (sourced by the scalar field) during the radiative epoch. For  $\rho_B \leq \rho_i \leq \rho_C$ , inflation is a transient, and the universe reverts to being radiation-dominated after the scalar field has fallen to smaller values. Larger initial values,  $\rho_i > \rho_C$ , result in a universe which inflates all the way until the present. For  $m = 10^{-22}$  eV, one finds  $\rho_B = 5.71 \times 10^{-26}$  GeV<sup>4</sup>,  $\rho_C = 1.71 \times 10^{-24}$  GeV<sup>4</sup>.

We therefore find that the potential (4.4) suffers from a severe fine-tuning problem since, for any given value of  $m$ , there is only a very narrow range of  $\varphi_i$  which will lead to currently admissible values of the matter density  $\Omega_{0m}$ . These results support the earlier findings of [14].<sup>4</sup>

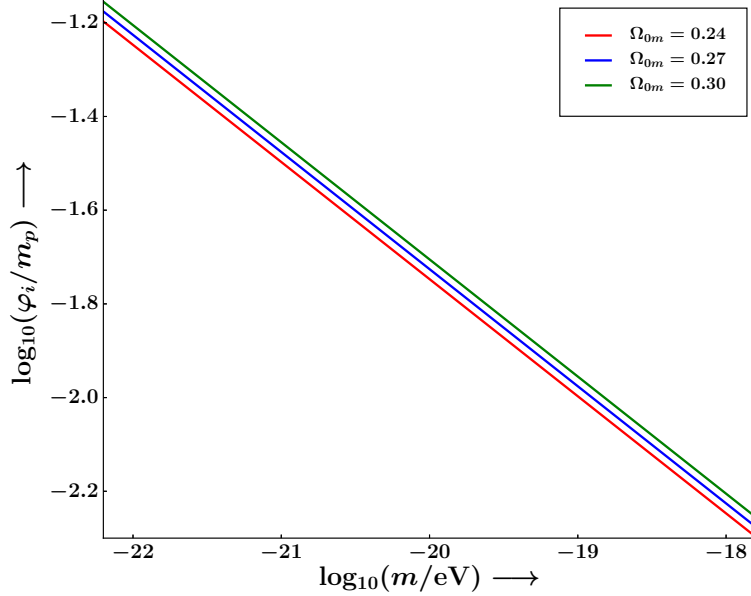


**Figure 3:** Dependence of the initial value  $\varphi_i$  of the scalar field on the mass  $m$  is shown for the scalar-field potential  $V(\varphi) = \frac{1}{2}m^2\varphi^2$ . Three different values of the present matter density parameter  $\Omega_{0m}$  are assumed. One sees that, for a given value of  $\Omega_{0m}$ , the value of  $\varphi_i$  decreases with increasing  $m$  according to the relation  $\varphi_i \propto m^{-1/4}$ . Consequently, for a fixed value of the mass  $m$ , larger values of  $\Omega_{0m}$  are associated with larger initial values of  $\varphi_i$ .

The foregoing analysis focused on a scalar field of mass  $m = 10^{-22}$  eV, which presents a lower bound on the mass of an oscillating scalar field purporting to play the role of dark matter [18]. However, it is important to study the effect of varying  $m$  on the initial field value  $\varphi_i$  and hence on the initial energy density  $\rho_i \simeq \frac{1}{2}m^2\varphi_i^2$ . It is straightforward to show that, if  $\varphi$  plays the role of dark matter, then  $\varphi_i$  scales with the mass as  $\varphi_i \propto m^{-1/4}$  (see Appendix C). In effect,

$$\varphi_i = 0.06 \times \left( \frac{m}{10^{-22} \text{ eV}} \right)^{-1/4} m_p. \quad (4.8)$$

<sup>4</sup>It is interesting to note that the fine tuning which we observe is insensitive to the initial value of  $\dot{\varphi}$ , as demonstrated in Figure 1.

Figure 3 illustrates this relationship for three different values of the current dark-matter density parameter  $\Omega_{0m}$ . Note that a larger value of  $\Omega_{0m}$  requires a larger initial value  $\varphi_i$  for a given scalar field mass  $m$ . The above result can easily be translated into a relationship between  $\rho_i$  and  $m$  using  $\rho_i \simeq \frac{1}{2}m^2\varphi_i^2$ .

## 4.2 Dark Matter from the *E-Model*

It is interesting that the extreme fine-tuning problem faced by the  $\frac{1}{2}m^2\varphi^2$  potential is easily alleviated if dark matter is based on the *E-model*. In this case, one can write down the potential (3.4) with  $n = 1$ , in the form

$$V(\varphi) = V_0 \left(1 - e^{-\lambda \frac{\varphi}{m_p}}\right)^2, \quad (4.9)$$

which closely resembles the Starobinsky model [7].

The potential (4.9) exhibits three asymptotic branches (see figure 4):

$$\text{Tracker wing: } V(\varphi) \simeq V_0 e^{2\lambda|\varphi|/m_p}, \quad \varphi < 0, \quad \lambda|\varphi| \gg m_p, \quad (4.10)$$

$$\text{Flat wing: } V(\varphi) \simeq V_0, \quad \lambda\varphi \gg m_p, \quad (4.11)$$

$$\text{Oscillatory region: } V(\varphi) \simeq \frac{1}{2}m^2\varphi^2, \quad \lambda|\varphi| \ll m_p, \quad (4.12)$$

where

$$m^2 = \frac{2V_0\lambda^2}{m_p^2}. \quad (4.13)$$

We note that the tracker parameter  $\lambda$  in the potential (4.9) is related to the geometric parameter  $\alpha$  in (3.4) by

$$\lambda = \sqrt{\frac{2}{3\alpha}}. \quad (4.14)$$

We now proceed to study the motion of the scalar field along the different branches (wings) of the *E-model* potential.

### 4.2.1 Evolution along the tracker wing

It is well known that that, in the context of Starobinsky inflation, only the flat wing of the potential sustains inflation since the tracker wing is much too steep to cause accelerated expansion. For dark matter, on the other hand, it is the steep wing with  $V \sim e^{2\lambda \frac{|\varphi|}{m_p}}$  that is more useful<sup>5</sup>. The reason for this has to do with the fact that a scalar field moving down a sufficiently steep potential can ‘track’ the cosmological background density [26–28]. In the case of the exponential potential (4.10), if  $\rho_r$  is the radiation density, then prior to matter-radiation equality, we have

$$\frac{\rho_\varphi}{\rho_{\text{total}}} = \frac{1}{\lambda^2} \quad (4.15)$$

where  $\rho_{\text{total}} = \rho_\varphi + \rho_r$ . Thus, a field rolling down the steep wing soon follows the common evolutionary path (4.15) from a wide range of initial conditions. This occurs so long as

<sup>5</sup>As mentioned earlier, the Starobinsky model of inflation corresponds to the choice  $\alpha = 1$  for which the left wing is not steep enough to provide tracking.

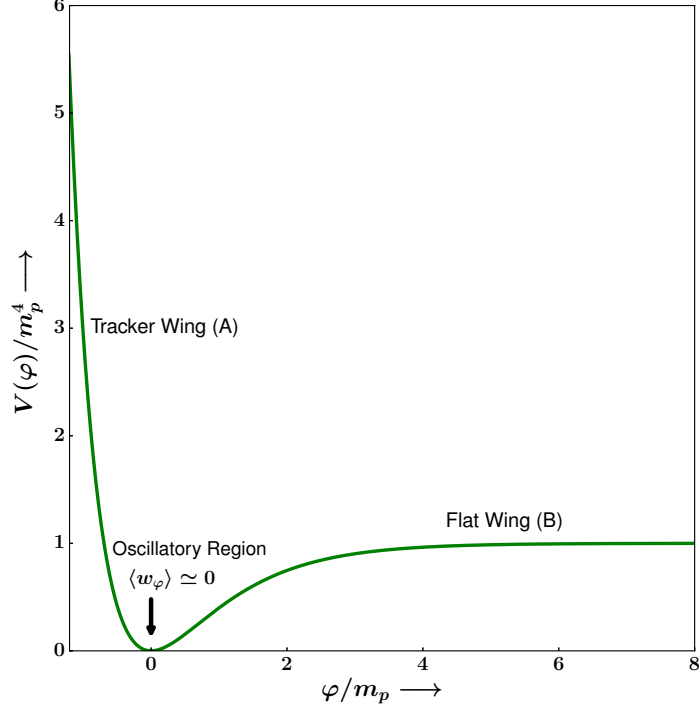


**Figure 4:** This figure schematically illustrates the *E-model* potential (4.9) with  $\lambda = 1$ . The main features of this potential are: the exponential tracker wing for  $\lambda|\varphi| \gg m_p$  ( $\varphi < 0$ ), the flat wing for  $\lambda\varphi \gg m_p$ , and the oscillatory region for which  $\lambda|\varphi| \ll m_p$ , so that  $V \simeq \frac{1}{2}m^2\varphi^2$ .

$\lambda|\varphi| \gg m_p$ . The scalar field begins to behave like dark matter, with  $\langle w \rangle \simeq 0$ , once  $\varphi$  has dropped to sufficiently small values and begins to oscillate. The following conditions must be satisfied for this to happen [8]:

$$\lambda|\varphi| \ll m_p, \quad m^2 \equiv V'' = \frac{2V_0\lambda^2}{m_p^2} = H^2(t_*). \quad (4.16)$$

This behaviour is illustrated in figure 5 for the parameter values  $\lambda = 14.5$  (corresponding to  $\alpha = 3.17 \times 10^{-3}$ ) and  $V_0 = 1.37 \times 10^{-28} \text{ GeV}^4$ . With these parameters, the effective mass of the scalar field is  $m \simeq 10^{-22} \text{ eV}$ , and the corresponding Jeans length is about a kiloparsec. The field begins to oscillate when  $m/H \sim 1$ , which corresponds to a redshift of  $z \sim 3 \times 10^6$ . Figure 5 demonstrates that the fine tuning in the initial scalar field energy density that existed for the  $m^2\varphi^2$  potential has been substantially removed. For the sake of completeness, we give below the initial energy-density values corresponding to:

- (i) the scaling attractor solution ( $P_2$  in figure 5):

$$\rho_{P_2} = 1.46 \times 10^{-13} \text{ GeV}^4, \quad (4.17)$$

- (ii) the maximum and minimum values of initial density that lead to  $\Omega_{0m} \simeq 0.27$ :

$$\begin{aligned} \rho_{\text{max}}(\equiv \rho_{P_3}) &= 6.47 \times 10^{-12} \text{ GeV}^4, \\ \rho_{\text{min}}(\equiv \rho_{P_1}) &= 3.05 \times 10^{-21} \text{ GeV}^4, \end{aligned} \quad (4.18)$$

which are related to the points  $P_1$  and  $P_3$  in figure 5.

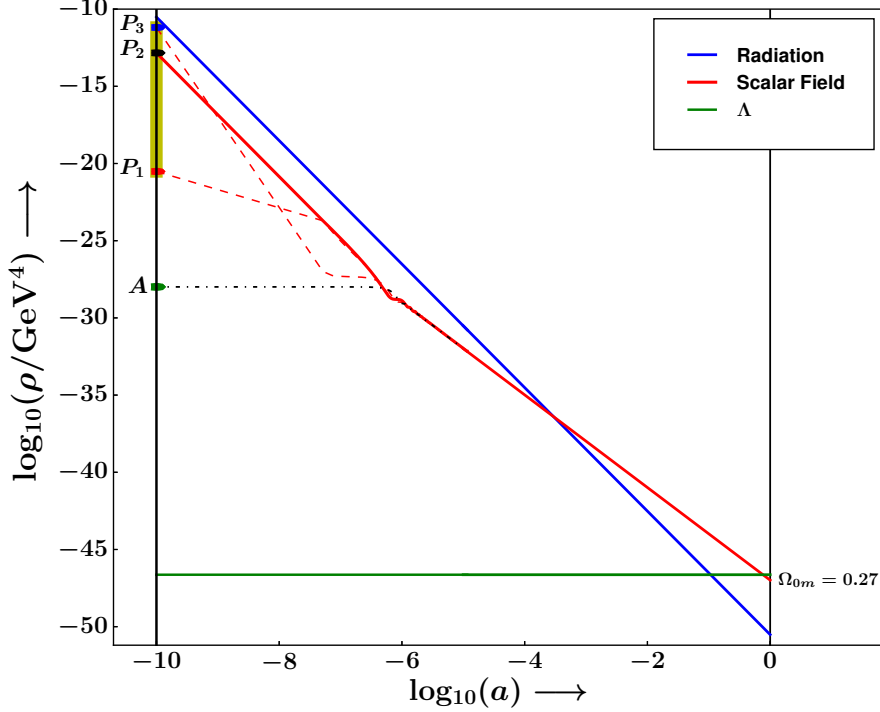


**Figure 5:** This figure describes the evolution of the scalar-field energy density from  $z \simeq 10^{10}$  until  $z = 0$ . The scalar field commences its descent from the steep left wing (‘A’ in figure 4) of the potential  $V(\varphi) = V_0 (1 - e^{-\lambda\varphi/m_p})^2$ . We have chosen  $\lambda = 14.5$  and  $V_0 = 1.37 \times 10^{-28} \text{ GeV}^4$ , which correspond to  $m = \frac{\sqrt{2V_0\lambda}}{m_p} \simeq 10^{-22} \text{ eV}$ . The band from  $P_1$  to  $P_3$  represents the range in the initial (scalar-field) energy density that leads to a reasonable value for the dark-matter density at the present epoch, namely  $\Omega_{0m} \simeq 0.27$ . Point  $P_2$  marks the initial energy density corresponding to the attractor solution (solid red line) to which all trajectories starting in the  $P_1$ – $P_3$  band converge (prior to the commencement of oscillations in  $\varphi$ ). This behaviour is in sharp contrast to that of dark matter sourced by the  $V(\varphi) = \frac{1}{2}m^2\varphi^2$  potential, for which only a very narrow finely tuned range of values of the initial energy density (around point A) lead to  $\Omega_{0m} \simeq 0.27$ . (For clarity of presentation, we do not show the baryon density.)

Our results, summarized in figure 5, demonstrate that initial energy-density values covering a range of more than 9 orders of magnitude at  $z = 10^{10}$  converge onto the attractor scaling solution which gives rise to  $\Omega_{0m} \simeq 0.27$  at present. This range substantially increases if we place our initial conditions at earlier times. For instance, if one sets  $\{\varphi, \dot{\varphi}\}$  at the GUT scale of  $10^{14} \text{ GeV}$  ( $z \sim 10^{26}$ ), then the range of initial density values that converge to  $\Omega_{0m} \simeq 0.27$  is an astonishing 82 orders of magnitude! The tracker branch of the *E-model* potential, therefore, allows a much greater freedom in the choice of initial conditions than the  $m^2\varphi^2$  potential. In particular it permits the possibility of equipartition, according to which the density in dark matter and radiation may have been comparable at very early times.

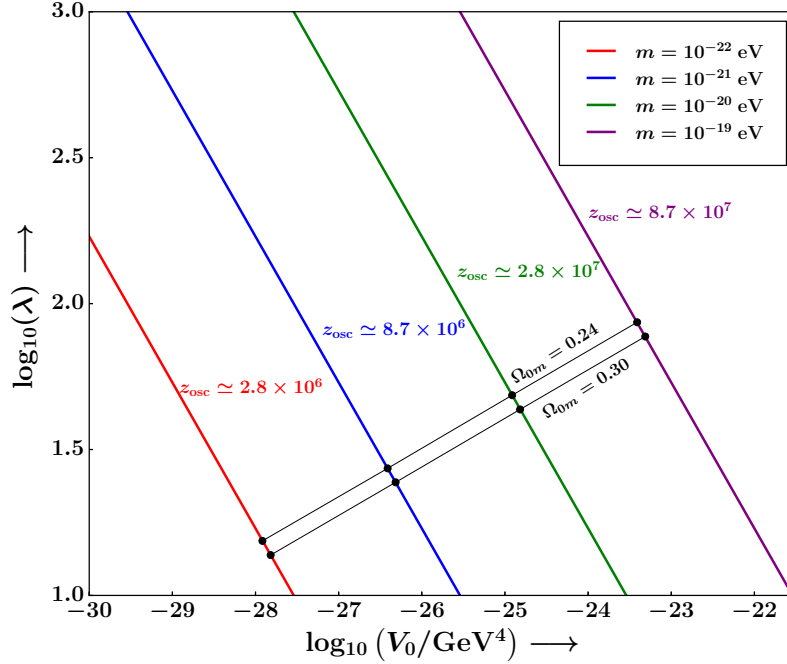


**Figure 6:** The tracker parameter  $\lambda = \frac{2}{\sqrt{6}\alpha}$  is plotted against  $V_0$  for the steep (tracker) wing of the  $E$ -model potential (4.9). The field begins to oscillate when  $m \sim H$  where  $m = \frac{\sqrt{2V_0}\lambda}{m_p}$ . An increase in mass therefore implies an increase in the redshift  $z_{\text{osc}}$  at which the scalar field begins to oscillate. Coloured parallel lines correspond to different values of  $m$  and  $z_{\text{osc}}$ . Values of  $\lambda$  and  $V_0$  which result in  $\Omega_{0m} \simeq 0.24$  and  $\Omega_{0m} \simeq 0.30$  are shown as parallel black lines. Their intersection with the coloured lines describing constant values of  $m$  and  $z_{\text{osc}}$  is marked by filled circles.

Our previous analysis focussed on a scalar field having an effective mass  $m = 10^{-22}$  eV. We chose this particular value of  $m$  since it could help resolve the cusp-core and substructure problems faced by standard cold dark matter (SCDM) [5, 18]. Although masses smaller than  $10^{-22}$  eV could be problematic for structure formation, larger values of  $m$  are by no means ruled out. Indeed, for  $m \gg 10^{-15}$  eV, our model becomes indistinguishable from SCDM. Since, in the  $E$ -model,  $m$  is a composite quantity, being related to  $\lambda$  and  $V_0$  through (4.2), it is of interest to determine a general relationship between  $\lambda = \frac{2}{\sqrt{6}\alpha}$  and  $V_0$  which would lead to the current value of the matter density. Such a relationship has been plotted in figure 6, in which values of  $V_0$  and  $\lambda$  giving rise to  $\Omega_{0m} = 0.24$  and  $0.30$  are shown as black lines. One should note that each point on either of these two lines refers to a family of initial conditions  $\{\varphi_i, \dot{\varphi}_i\}$  which get funneled onto a given  $\Omega_{0m}$  by means of the attractor mechanism described in figure 5.

#### 4.2.2 Evolution along the flat wing

Next, we explore the possibility of obtaining dark matter from the flat right wing of the  $E$ -model potential (4.11). (It is this wing which is responsible for generating inflation in the Einstein frame of the Starobinsky model.) Note that the value of  $V_0$  sets the height of the flat wing of the potential in figure 4. The fact that the effective mass of the scalar field depends

upon  $V_0$  through  $m = \sqrt{2V_0}\lambda/m_p$  opens up several different possibilities for initial values of the scalar field. For instance, if  $m$  is held fixed at  $10^{-22}$  eV and the values of  $\lambda$  and  $V_0$  are chosen in conformity with our previous analysis, namely  $\lambda = 14.5$  and  $V_0 = 1.37 \times 10^{-28} \text{ GeV}^4$ , then our results, shown in figure 7, demonstrate that, as in the case of the  $m^2\varphi^2$  potential, one encounters here a considerable fine tuning of initial conditions.

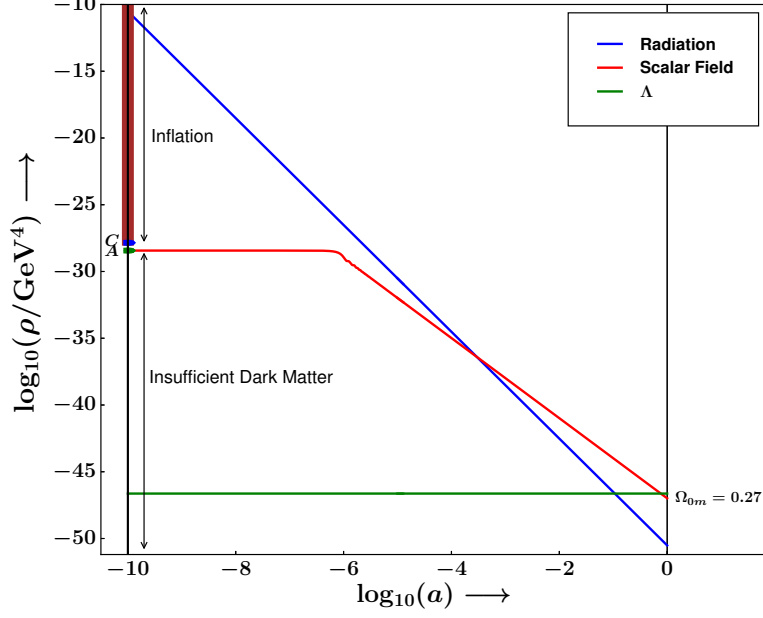


**Figure 7:** This figure describes the possibility that the scalar field associated with dark matter could have commenced rolling from the flat right wing (see figure 4) of the potential  $V(\varphi) = V_0 \left(1 - e^{-\lambda \frac{\varphi}{m_p}}\right)^2$ . We assume the same units as in figure 5, namely  $\lambda = 14.5$  and  $V_0 = 1.37 \times 10^{-28} \text{ GeV}^4$  which correspond to  $m \simeq 10^{-22} \text{ eV}$ . The energy densities (in units of  $\text{GeV}^4$ ) of radiation and scalar field are plotted against the scale factor  $a$ . We notice that the scalar-field energy density remains pegged to its initial value when the radiation energy density is large. Subsequently, the radiation energy density drops, which decreases the damping in the scalar-field equation of motion (4.7). From this point onwards ( $z \sim 10^6$ ), the scalar field is free to move and to oscillate. Consequently, from here on it behaves like dark matter. Point A describes the (fine-tuned) initial value of the scalar-field energy density which leads to  $\Omega_{0m} \simeq 0.27$ . The brown band pointing upwards from point C shows the range of initial values which drive the universe into an inflationary accelerating phase which lasts until the present epoch. Small initial values  $\rho_i \ll \rho_A$  lead to an insufficient amount of dark matter at present. (For clarity of presentation, we do not show the baryon density.)

For instance, the fine-tuned initial value of the scalar field density which ensures  $\Omega_{0m} = 0.27$ , is given by  $\rho_A = 3.68 \times 10^{-29} \text{ GeV}^4$ . If the initial energy density of the scalar field is larger than  $\rho_B = 1.32 \times 10^{-28} \text{ GeV}^4$ , then the universe enters into an accelerating (inflationary) phase. For values of the initial energy density between  $\rho_B$  and  $\rho_C = 1.37 \times 10^{-28} \text{ GeV}^4$ , the accelerating phase is a transient, whereas for initial energy-density values larger than  $\rho_C = 1.37 \times 10^{-28} \text{ GeV}^4$  (brown band in figure 7) the inflationary phase lasts until the

present epoch. As in the case of the  $m^2\varphi^2$  potential, initial energy-density values smaller than  $\rho_A$  result in an insufficient amount of dark matter at the current epoch. (Note that the values of  $\rho_B$  and  $\rho_C$  are much too close to be distinguished in figure 7.) We therefore conclude that the flat right wing of the *E-model* potential with  $\lambda = 14.5$ ,  $V_0 = 1.37 \times 10^{-28} \text{ GeV}^4$  and  $m = 10^{-22} \text{ eV}$  suffers from a fine-tuning problem similar to the one which afflicts the  $m^2\varphi^2$  potential.

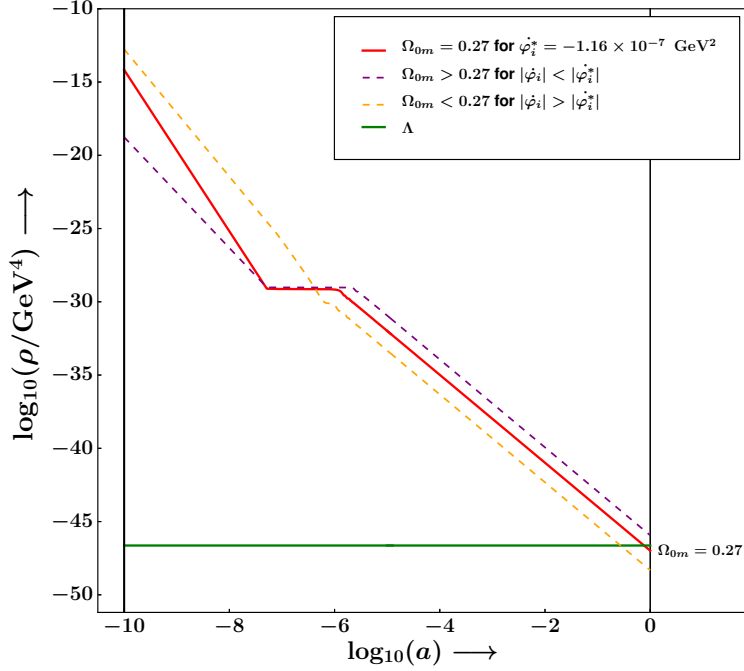


**Figure 8:** This figure illustrates the importance of the initial velocity  $\dot{\varphi}_i$  in determining the extent of dark matter at the present epoch. Again, the scalar field rolls down the flat right wing of the *E-model* potential (4.9). The height of the potential is now somewhat lower than that in figure 7, namely  $V_0 = 10^{-29} \text{ GeV}^4$ . Again,  $m = 10^{-22} \text{ eV}$  with  $\lambda$  determined from (4.2). The comparatively lower value of  $V_0$  allows the field to commence rolling from on top of the flat potential where  $V' \simeq 0$ . One finds that, for the initial value  $\varphi_i = 7.35 \times 10^{-2} m_p$ , only a highly fine-tuned value of  $\dot{\varphi}_i = \dot{\varphi}_i^*$  results in the correct value of the dark-matter density today, namely  $\Omega_{0m} \simeq 0.27$  (red curve). Slight deviations from this value of  $\dot{\varphi}_i$  result either in an overdensity of  $\Omega_{0m} > 0.27$  (purple dashed line) or in an underdensity  $\Omega_{0m} < 0.27$  (orange dashed line). (For clarity of presentation, we do not show the radiation and baryon energy density.)

Note that the location of the initial value  $\varphi_i$  on the flat wing can be crucial in determining the fate of the universe. For instance, if  $\varphi_i$  is large enough to place the field on top of the flat wing where  $V' \simeq 0$ , then the equation of motion (4.7) simplifies to  $\ddot{\varphi} + 3H\dot{\varphi} \simeq 0$ , which has the solution  $\dot{\varphi} \propto a^{-3}$ . Thus  $\varphi$  can grind to a halt en-route to the minimum of the potential. In this case, if the initial value  $\varphi_i$  is large and if  $\dot{\varphi}_i^2 \ll V_0$ , then the kinetic term will decay completely while  $\varphi$  is still on the flat wing. This can lead to eternal inflation. This problem can be avoided if  $\varphi_i$  is not too large, and if  $(\dot{\varphi}^2)_i \gg V_0$ . The effect of varying the initial



scalar-field velocity  $\dot{\varphi}_i$  on the current dark-matter density is shown in figure 8. We start with a moderate initial value  $\varphi_i = 7.35 \times 10^{-2} m_p$ , which ensures that the field does not commence rolling from too far along the flat wing, and thereby avoids the problem of eternal inflation. We then vary  $\dot{\varphi}_i$  for a potential with  $V_0 = 10^{-29} \text{ GeV}^4$ . (The corresponding value of  $\lambda$  is determined from (4.2) assuming  $m = 10^{-22} \text{ eV}$ .) The value of  $\dot{\varphi}_i$  which gives rise to  $\Omega_{0m} = 0.27$  is given by  $\dot{\varphi}_i^* = -1.16 \times 10^{-7} \text{ GeV}^2$  (red line). Smaller values of  $\dot{\varphi}_i$  delay the onset of oscillations in the scalar field. This leads to a larger value of the dark-matter density at the present epoch,  $\Omega_{0m} > 0.27$  (purple dashed line). A larger initial kinetic term has the opposite effect of making the scalar field oscillate earlier, which results in a smaller value of the dark-matter density,  $\Omega_{0m} < 0.27$  (orange dashed line).

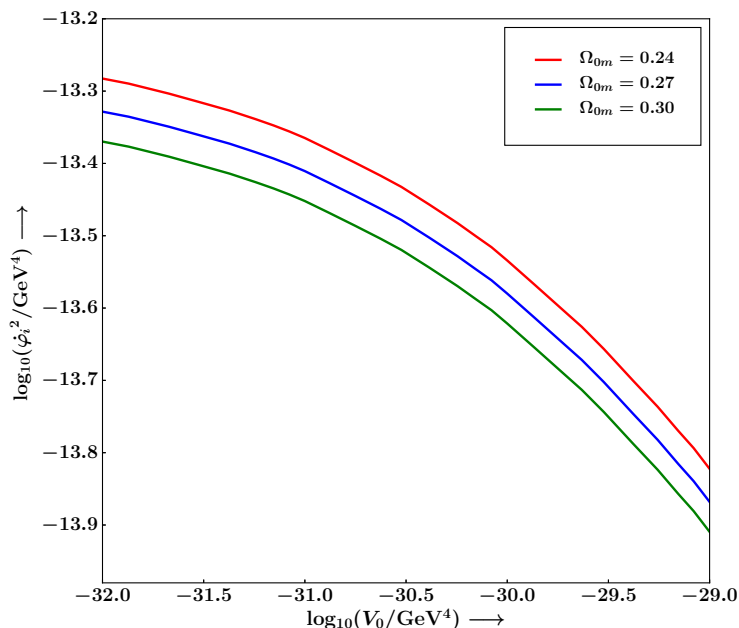


**Figure 9:** Values of  $\dot{\varphi}_i^2$  and  $V_0$  resulting in  $\Omega_{0m} \simeq 0.24, 0.27$ , and  $0.30$  are shown. Note that  $V_0$  describes the height of the flat wing of the potential in (4), and that larger values of  $\dot{\varphi}_i^2$  correlate with smaller values of  $V_0$  for a given  $\Omega_{0m}$ .

The dependence of the initial kinetic term  $\dot{\varphi}_i^2$  on the height  $V_0$  of the flat wing has been numerically analyzed with the initial field value held fixed at  $\varphi_i = 7.35 \times 10^{-2} m_p$ . Our results are shown in figure 9. We find that smaller values of  $V_0$  require larger values of  $\dot{\varphi}_i^2$  in order to give the same final value of  $\Omega_{0m}$ . This correlation is expected since one obeys the mass relation (4.2) while varying the height  $V_0$  of the potential. For smaller  $V_0$  values, an initial  $\varphi_i = 7.35 \times 10^{-2} m_p$  sits *further along* on the flat wing of the potential (see figure 10). Hence the field requires a larger initial velocity  $\dot{\varphi}_i$  in order to start oscillating at the correct epoch ( $z_{\text{osc}} \sim 10^6$  for  $m = 10^{-22} \text{ eV}$ ) thereby ensuring  $\Omega_{0m} = 0.27$ .

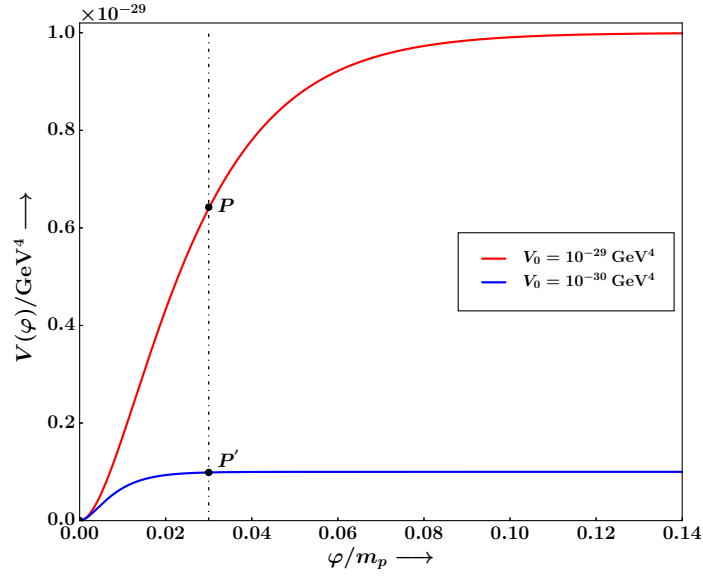


**Figure 10:** The right wing of the *E-model* potential  $V(\varphi)$  is shown for two values of  $V_0$ . Notice that, for a lower potential (blue), the initial value  $\varphi_i$  is associated with a point  $P'$  located along the *flat wing* of  $V(\varphi)$ . By contrast, the same value of  $\varphi_i$  is associated with the *steep wing*  $P$  of the higher potential (red).

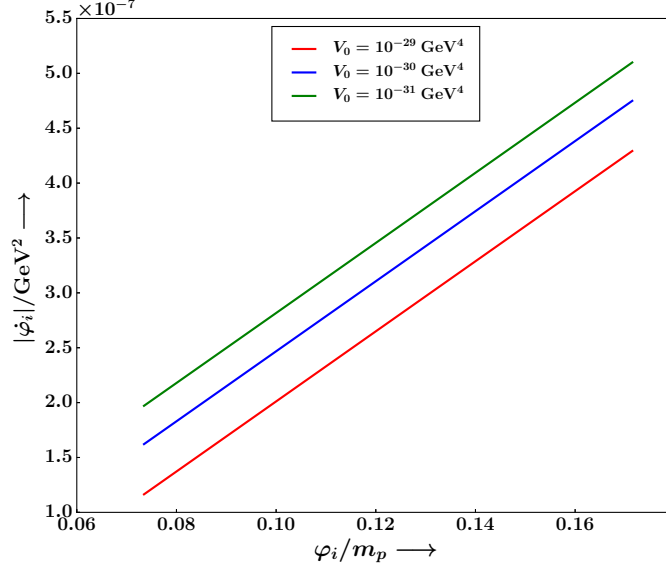


**Figure 11:** The initial velocity  $\dot{\varphi}_i$  which results in  $\Omega_{0m} = 0.27$  is plotted as a function of  $\varphi_i$  for three different values of the potential height  $V_0$ . Notice that, for a given  $V_0$ , a larger value of  $\varphi_i$  implies a larger  $|\dot{\varphi}_i|$ . However, if  $\varphi_i$  is held fixed, then  $|\dot{\varphi}_i|$  decreases with increasing  $V_0$ , in agreement with figure 9.

As might be expected, for a fixed value of  $V_0$ , the initial velocity  $\dot{\varphi}_i$  required to achieve a

given value of  $\Omega_{0m}$  increases with an increase in the initial field value  $\varphi_i$ .<sup>6</sup> This is illustrated in figure 11 which also shows that the dependence of  $\dot{\varphi}_i$  on  $\varphi_i$  is linear.

### 4.3 Dark Matter from the Tracker Model

For  $n = 1$ , the tracker potential (3.5) can be written as

$$V(\varphi) = V_0 \sinh^2 \frac{\lambda \varphi}{m_p}, \quad (4.19)$$

where the parameter  $\lambda$  is related to the geometric parameter  $\alpha$  in (3.5) by

$$\lambda = \sqrt{\frac{2}{3\alpha}}. \quad (4.20)$$

This symmetric potential has the following branches (see figure 12):

$$\text{Two tracker wings: } V(\varphi) \simeq V_0 e^{2\frac{\lambda|\varphi|}{m_p}}, \quad \lambda|\varphi| \gg m_p, \quad (4.21)$$

$$\text{Oscillatory region: } V(\varphi) \simeq \frac{1}{2}m^2\varphi^2, \quad \lambda|\varphi| \ll m_p, \quad (4.22)$$

where  $m^2 = 2V_0\lambda^2/m_p^2$  and the relation between the tracker parameter  $\lambda$  and the geometric parameter  $\alpha$  is given by (4.14).

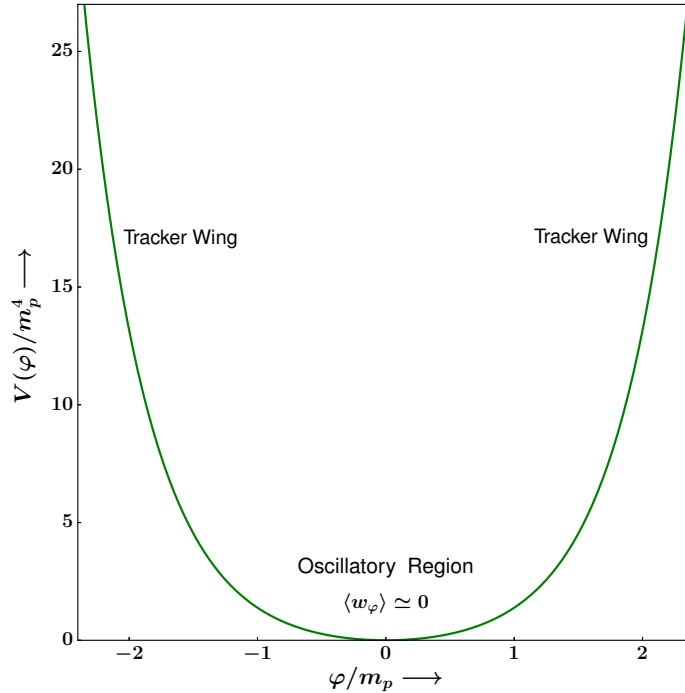


**Figure 12:** This figure schematically illustrates the tracker potential (4.19). The asymptotic tracker wings correspond to  $\lambda|\varphi| \gg m_p$ , while, for  $\lambda|\varphi| \ll m_p$ , we have  $V(\varphi) \simeq \frac{1}{2}m^2\varphi^2$ .

<sup>6</sup>We only consider fields rolling towards the minimum of the potential, since a field moving in the opposite direction will give rise to eternal inflation for all values of  $\dot{\varphi}_i$ .

The potential (4.19) converges to an exponential for large values of  $\lambda|\varphi|$ . It therefore has much in common with the left wing of the *E-model* potential (3.4). The evolution of energy densities in radiation, a cosmological constant and the scalar field is shown in figure 13 for parameter values  $\lambda = 48.93$  (corresponding to  $\alpha = 2.78 \times 10^{-4}$ ) and  $V_0 = 1.20 \times 10^{-25} \text{ GeV}^4$ , which correspond to  $m = 10^{-20} \text{ eV}$ . For this value of  $m$ , the scalar field begins to oscillate at  $z \sim 3 \times 10^7$ .

The tracker-like properties of this potential, shown in figure 13, ensure that initial density values covering a range of almost 6 orders of magnitude (at  $z = 10^{10}$ ), converge onto the attractor scaling solution which gives  $\Omega_{0m} \simeq 0.27$ . This range covers more than 73 orders of magnitude if one sets initial conditions at the GUT scale of  $10^{14} \text{ GeV}$  ( $z \sim 10^{26}$ ).

The initial energy-density value corresponding to the scaling attractor solution  $P_2$  in figure 13 is  $\rho_{P_2} = 1.28 \times 10^{-14} \text{ GeV}^4$ . The maximum and minimum values of the initial energy density that lead to  $\Omega_{0m} \simeq 0.27$  are given by

$$\begin{aligned}\rho_{\max}(\equiv \rho_{P_3}) &= 2.65 \times 10^{-12} \text{ GeV}^4, \\ \rho_{\min}(\equiv \rho_{P_1}) &= 3.05 \times 10^{-18} \text{ GeV}^4.\end{aligned}\tag{4.23}$$

These are related, respectively, to the points  $P_1$  and  $P_3$  in figure 13.

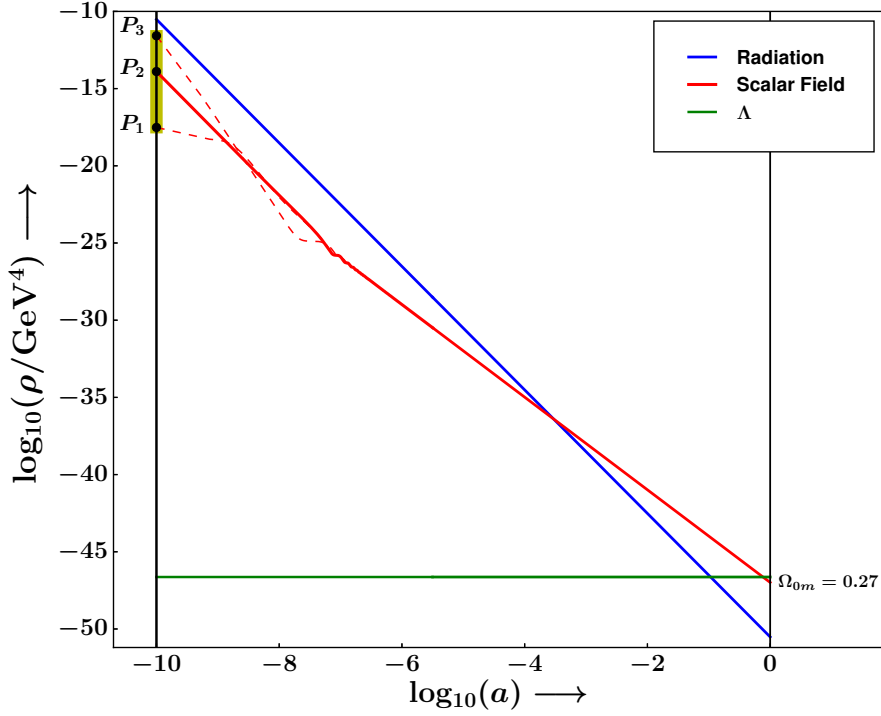


**Figure 13:** This figure describes the evolution of the density in a scalar field which commences its descent from one of the steep tracker wings of  $V(\varphi) = V_0 \sinh^2 \frac{\lambda\varphi}{m_p}$  at  $z \simeq 10^{10}$ . We choose  $\lambda = \frac{2}{\sqrt{6\alpha}} = 48.9$  and  $V_0 = 1.2 \times 10^{-25} \text{ GeV}^4$  so that  $m = \frac{\sqrt{2V_0}\lambda}{m_p} \simeq 10^{-20} \text{ eV}$ . The band from  $P_1$  to  $P_3$  represents the range in the initial energy-density values which converge to  $\Omega_{0m} \simeq 0.27$  at present.  $P_2$  denotes the initial density corresponding to the attractor solution (solid red line) to which all trajectories starting on the  $P_1$ – $P_3$  band converge prior to the commencement of oscillations. (For clarity of presentation, we do not show the baryon density.)

The relationship between  $\lambda$  and  $V_0$  is similar to that shown in figure 6 for the steep wing of the *E-model*, therefore we do not show it here. Because of the presence of symmetric tracker wings, this model is perhaps the most robust of the three  $\alpha$ -attractor potentials we have considered in providing a scalar-field description of dark matter.

#### 4.4 Dark Matter from the T-Model

The T-model potential (3.6) with  $n = 1$  becomes

$$V(\varphi) = V_0 \tanh^2 \lambda_1 \frac{\varphi}{m_p} \quad (4.24)$$

where the potential parameter  $\lambda_1$  is related to the geometric parameter  $\alpha$  by

$$\lambda_1 = \frac{1}{\sqrt{6\alpha}} \quad (4.25)$$

This potential is characterized by two asymptotically flat regions and an intermediate region in which, for  $\lambda_1|\varphi| \ll 1$ , the potential behaves like  $m^2\varphi^2$  (see figure 14). In other words,

$$\begin{aligned} \text{for } \lambda_1|\varphi| \gg m_p, \quad V(\varphi) &\simeq V_0, \quad (\text{flat wings}), \\ \text{for } \lambda_1|\varphi| \ll m_p, \quad V(\varphi) &\simeq \frac{1}{2}m^2\varphi^2, \end{aligned} \quad (4.26)$$

where  $m^2 = 2V_0\lambda_1^2/m_p^2$ .

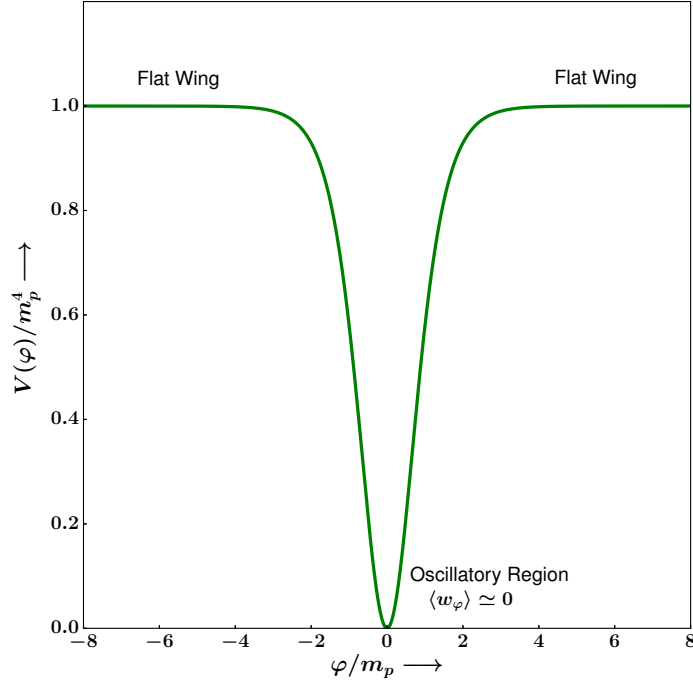


**Figure 14:** This figure schematically shows the T-model potential (4.24). This potential is characterized by two asymptotically flat wings (for  $\lambda_1|\varphi| \gg m_p$ ) and an intermediate region in which  $V \sim m^2\varphi^2$  (for  $\lambda_1|\varphi| \ll m_p$ ).

Clearly, the flat wings of this potential are very similar to the flat right wing of the *E-model* potential (4.9). Consequently the analysis for this model is qualitatively similar to that done in section 4.2.2. As in that case, the initial velocity  $\dot{\varphi}_i$  plays an important role in determining the value of the current matter density  $\Omega_{0m}$ . We do not repeat this analysis here, referring instead the reader to figures 7, 8, 9, 10 and 11 for details. One might note that, because of the absence of an exponential tracker wing in (4.24), the initial conditions which give rise to a realistic construct for dark matter in the T-model are less generic than those discussed in the previous section 4.3 for the tracker model.

#### 4.5 Gravitational Instability

We demonstrated in the previous section that dark matter based on  $\alpha$ -attractors could emerge from a much larger class of initial conditions than admitted by the canonical model  $\frac{1}{2}m^2\varphi^2$ .

It is well known that a coherently oscillating scalar field experiences gravitational instability [29]. In the case of the canonical model the associated Jeans wavenumber given by [11, 15]

$$k_J^2 = \sqrt{2\rho} \frac{m}{m_p} . \quad (4.27)$$

For small values of  $m$ , the large Jeans length associated with ultra-light (fuzzy) dark matter might help resolve several shortcomings of standard CDM including the cusp-core problem, the substructure problem, etc. (see [18] for a recent review). It therefore becomes important to determine the Jeans length associated with the  $\alpha$ -attractor family of dark-matter models (4.9), (4.19) and (4.24). This shall be the purpose of the present section.

One first notes that, for small values of  $\varphi$ , the potentials corresponding to tracker dark matter (4.19), and the T-model (4.24) acquire a form similar to that of the anharmonic oscillator

$$V(\varphi) = \frac{1}{2}m^2\varphi^2 + \frac{1}{4}\lambda_0\varphi^4 . \quad (4.28)$$

Gravitational instability in such a potential was analyzed in [11, 30] in the limit  $\lambda_0\varphi^2 \ll m^2$ . Employing the theory of parametric resonance (see Appendix A for details), one obtains the following expression for the Jeans scale ( $k_J = 2\pi/\lambda_J$ ):

$$k_J^2 = -\frac{9}{8}\lambda_0\varphi_0^2 + \sqrt{\left(\frac{9}{8}\lambda_0\varphi_0^2\right)^2 + \frac{m^4\varphi_0^2}{m_p^2}} , \quad (4.29)$$

equivalently

$$k_J^2 = -\frac{9}{4}\lambda_0\frac{\rho}{m^2} + \sqrt{\left(\frac{9}{4}\lambda_0\frac{\rho}{m^2}\right)^2 + 2\rho\frac{m^2}{m_p^2}} , \quad (4.30)$$

where one notes that  $\rho = \frac{1}{2}m^2\varphi_0^2$ , with  $\varphi_0$  being the maximum amplitude of an oscillation. As expected, (4.29) reduces to (4.27) for  $\lambda_0 = 0$ .

For small values,  $\lambda_1|\varphi| \ll m_p$ , the T-model potential (4.24) reduces to

$$V(\varphi) \simeq V_0 \left[ \left( \lambda_1 \frac{\varphi}{m_p} \right)^2 - \frac{2}{3} \left( \lambda_1 \frac{\varphi}{m_p} \right)^4 \right] . \quad (4.31)$$

Comparing (4.31) with (4.28) one finds

$$m^2 = \frac{2V_0\lambda_1^2}{m_p^2} , \quad \lambda_0 = -\frac{8}{3} \frac{V_0\lambda_1^4}{m_p^4} . \quad (4.32)$$

We note that  $\lambda_1$  is related to  $\alpha$  by (4.25). Substituting (4.32) into (4.29) and using  $\rho = \frac{1}{2}m^2\varphi^2$ , gives the Jeans scale in the T-model (4.24)

$$k_J^2 = 3\frac{\lambda_1^2\rho}{m_p^2} + \left[ \left( 3\frac{\lambda_1^2\rho}{m_p^2} \right)^2 + 2\rho\frac{m^2}{m_p^2} \right]^{1/2} . \quad (4.33)$$

Note that  $\lambda_1$  is not a free parameter since it enters into the definition of  $m^2$  in (4.32).

For small values of  $\varphi$  the axion potential (4.1) also has the anharmonic form (4.28) with

$$m^2 = \frac{V_0}{f^2}, \quad \lambda_0 = -\frac{1}{6} \frac{m^2}{f^2}. \quad (4.34)$$

Substituting this in (4.29) gives the Jeans scale in the axion model

$$k_J^2 = \frac{3\rho}{8f^2} + \left[ \left( \frac{3\rho}{8f^2} \right)^2 + 2\rho \frac{m^2}{m_p^2} \right]^{1/2}. \quad (4.35)$$

Comparing (4.35) with (4.33), one finds a close affinity between the axion and the T-model, with (4.35) reverting to (4.33) after setting  $1/8f^2 = \lambda_1^2$ ; also see [30].

Next consider tracker dark matter. The potential (4.19) in the limit  $\lambda\varphi \ll 1$  takes the form

$$V(\varphi) \simeq V_0 \left[ \left( \frac{\lambda\varphi}{m_p} \right)^2 + \frac{1}{3} \left( \frac{\lambda\varphi}{m_p} \right)^4 \right]. \quad (4.36)$$

Comparing with (4.28), one finds

$$m^2 = \frac{2V_0\lambda^2}{m_p^2}, \quad \lambda_0 = \frac{4}{3} \frac{V_0\lambda^4}{m_p^4}, \quad (4.37)$$

and substitution in (4.29) gives the Jeans scale in the Tracker model (4.19)

$$k_J^2 = -\frac{3}{2}\lambda^2\rho + \left[ \left( \frac{3}{2}\lambda^2\rho \right)^2 + \rho \frac{m^2}{m_p^2} \right]^{1/2}, \quad (4.38)$$

where  $\rho = \frac{1}{2}m^2\varphi_0^2$ . Note that  $\lambda$  is not a free parameter since it enters into the definition of  $m^2$  in (4.37).

Finally, let us consider the small argument limit of the *E-model* potential (4.9)

$$V(\varphi) \simeq V_0 \left[ \left( \frac{\lambda\varphi}{m_p} \right)^2 - \left( \frac{\lambda\varphi}{m_p} \right)^3 + \frac{7}{12} \left( \frac{\lambda\varphi}{m_p} \right)^4 \right]. \quad (4.39)$$

This potential does not subscribe to the form (4.28) since it contains a cubic term in  $\varphi$ . As shown in Appendix A, the Jeans scale in this model is given by

$$k_J^2 = \left( \frac{5}{3} \frac{\mu^2\rho}{m^4} - \frac{9}{4} \frac{\lambda_0\rho}{m^2} \right) + \left[ \frac{2m^2}{m_p^2}\rho + \left( \frac{25}{9} \frac{\mu^4}{m^8} + \frac{81}{16} \frac{\lambda_0^2}{m^4} - \frac{15}{2} \frac{\lambda_0\mu^2}{m^6} \right) \rho^2 \right]^{\frac{1}{2}}. \quad (4.40)$$

Note that  $\mu, \lambda_0$  and  $m$  are not free parameters since they are related through  $m^2 = \frac{2V_0\lambda^2}{m_p^2}$ ,  $\mu = \frac{3\lambda^3 V_0}{m_p^3}$ ,  $\lambda_0 = \frac{7}{3} \frac{\lambda^4 V_0}{m_p^4}$ . The fundamental parameters in this model are  $V_0$  and  $\lambda = \sqrt{\frac{2}{3\alpha}}$ , with  $\alpha$  defined in section 3.

The expression for  $k_J^2$  in each of the three  $\alpha$ -dark matter models ( $\alpha$ DM) considered by us, namely (4.33), (4.38) and (4.40), contains terms proportional to  $\rho$  and  $\rho^2$  (under a common square root). By contrast, in the canonical  $m^2\varphi^2$  model,  $k_J^2$  is simply proportional to  $\sqrt{\rho}$ , see (4.27). Since  $\rho^2$  falls off faster than  $\rho$  during expansion, it is important to study



the evolution of  $k_J^2$  in all of these dark matter models. This has been done in figure 15, which shows  $k_J^2$  for the canonical  $m^2\varphi^2$  model with  $m = 10^{-22}$  eV, the tracker model and the  $E$ -model (both with  $\lambda = 14.5$ ). This figure shows that  $k_J^2$  in all three models converges to the expression (4.27) at late times by  $z \sim 10^3$ .

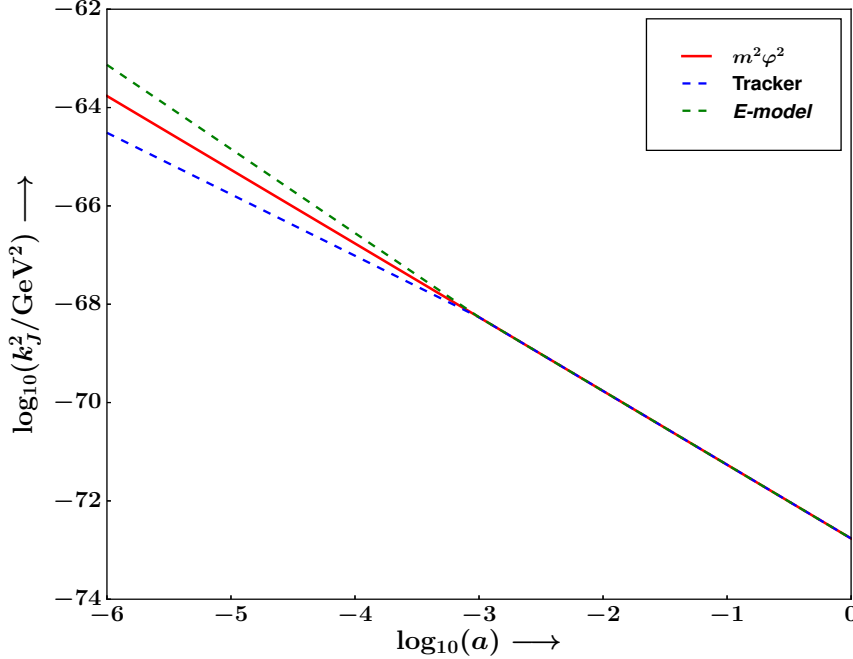


**Figure 15:** The evolution of the Jeans wavenumber  $k_J^2$  is shown for the quadratic potential (4.27) with  $m = 10^{-22}$  eV (red curve), the Tracker model (4.38) (blue curve) and the asymmetric  $E$ -model model (4.40) (green curve). (In the Tracker and  $E$  models  $\lambda = 14.5$  which ensures  $m = 10^{-22}$  eV. Note that, for a given value of  $m$ , only very fine-tuned values of  $\lambda$  ensure  $\Omega_{0m} \sim 0.27$ , as shown in figure 6.) We observe that  $k_J^2$  converges to the same value in all three dark-matter models by  $z \sim 10^3$ . For larger values of  $m$ , this convergence will occur at higher redshifts.

Another illustration of the result discussed above is depicted in figure 16 which shows the fractional difference in  $k_J^2$ ,

$$\frac{\Delta k_J^2}{k_J^2} = \frac{k_J^2|_{\alpha\text{DM}} - k_J^2|_{m^2\varphi^2}}{k_J^2|_{m^2\varphi^2}}, \quad (4.41)$$

between the Tracker model and the  $E$ -model on the one hand, and the  $m^2\varphi^2$  model on the other. Figures 15 and 16 demonstrate that the expression for the Jeans scale in the  $m^2\varphi^2$  model, namely (4.27), amply suffices to describe  $k_J^2$  also in the Tracker and  $E$  models for  $z < 10^3$ .

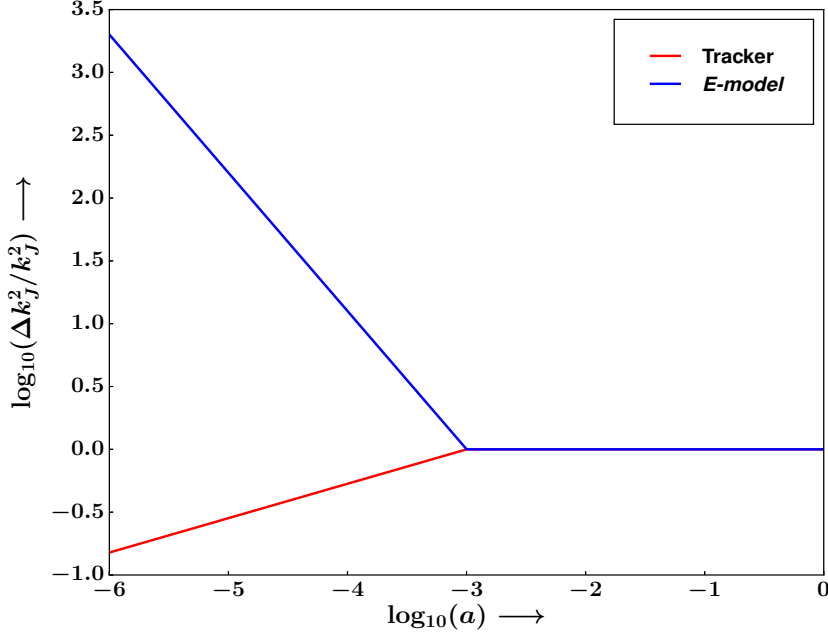


**Figure 16:** This figure shows the fractional difference between  $k_J^2$  in the tracker model (4.38) (red curve) and the  $E$ -model (4.40) (blue curve) on the one hand, and  $k_J^2$  in the  $m^2\varphi^2$  model (4.27) on the other ( $m = 10^{-22}$  eV is assumed). Note that the fractional difference  $\Delta k_J^2/k_J^2$  between the models becomes extremely small by redshift  $z \sim 10^3$ , after which the clustering properties of the tracker and  $E$  models become indistinguishable from those of the quadratic potential. For larger values of  $m$ , the value of  $\Delta k_J^2/k_J^2$  drops to zero at higher redshifts.

Next we turn to the T-model (3.6). In this case, one notes that there is no bound on the values of  $\lambda_1$  and  $V_0$  as long as the mass constraint relation (4.2) is satisfied. However, the expression for the Jeans scale in this model, namely (4.33), was derived under the assumption that the harmonic limit,  $\lambda_1\varphi^2 \ll m^2$ , is valid. This helps place an upper limit on  $\lambda_1$ , namely  $\lambda < 71$  if  $m \simeq 10^{-22}$  eV. In figure 17, the Jeans scale  $k_J^2$  for the T-model is shown as a function of the scale factor. This figure shows that the expressions for  $k_J^2$  in the T-model and  $m^2\varphi^2$  model converge for  $z < 10^3$  (assuming identical values of  $m$  in the two models). We therefore conclude that, in all of the  $\alpha$ -dark matter models discussed by us, the Jeans scale converges to that in the  $m^2\varphi^2$  model, namely (4.27), by  $z \sim 10^3$ .

One also needs to draw attention to the following point. In all our dark matter models, the scalar field begins to oscillate when  $m/H \sim 1$ . In other words, the scalar field can commence oscillating (and become pressureless) once the expansion rate  $H$  has dropped below the scalar field mass  $m$ . Prior to this, the behaviour of  $\varphi(t)$  depends upon the form of the potential. For the canonical potential  $V = \frac{1}{2}m^2\varphi^2$ , the equation of state of the scalar field is  $w_\varphi \simeq -1$  at early times. In the case of tracker dark matter,  $w_\varphi \simeq 1/3$  during the tracking phase, prior to the onset of oscillations. The EOS of matter during the pre-oscillatory epoch is likely to affect the power spectrum of dark matter perturbations. This is an important open problem to which we wish to return in a companion paper.

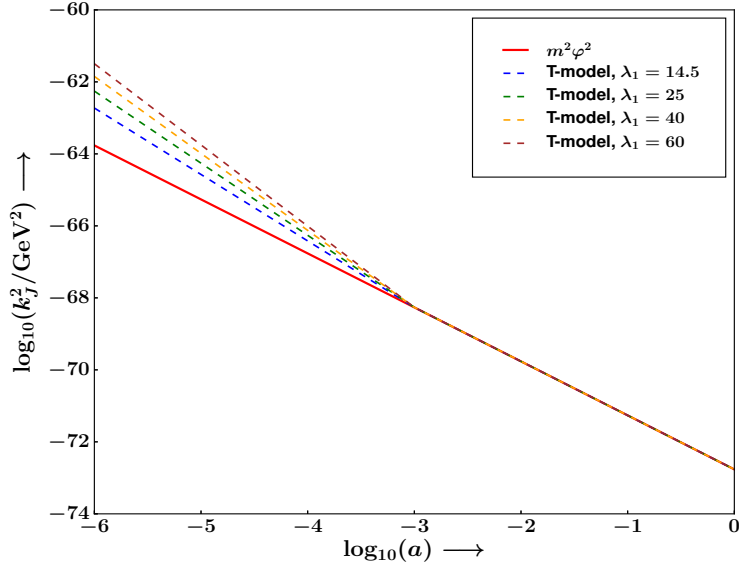


**Figure 17:** The Jeans wavenumber  $k_J^2$  for the T-model (4.33) and the quadratic potential (4.27) is shown as a function of  $\log_{10} a$  for five different values of  $\lambda$ . We find that, for all values of  $\lambda_1$ , the clustering scale in the T-model converges to that in the model with  $m^2\varphi^2$  potential by  $z \sim 10^3$ . Note that  $m = 10^{-22}$  eV in all models.

## 5 Dark Energy

### 5.1 Dark Energy from the potential $V \propto |\varphi|^{2n}$

The canonical potential<sup>7</sup> for oscillatory dark energy is given by

$$V(\varphi) = V_0 \left| \frac{\varphi}{m_p} \right|^{2n}, \quad n < \frac{1}{2}. \quad (5.1)$$

Once  $\varphi$  commences oscillating around  $\varphi = 0$ , its time-averaged equation of state becomes<sup>8</sup>

$$\langle w_\varphi \rangle = \frac{n-1}{n+1}. \quad (5.2)$$

The oscillating scalar field can drive cosmic acceleration when  $\langle w_\varphi \rangle < -1/3$ , which corresponds to  $n < 1/2$ . However, as we shall soon show, the initial density of the scalar field requires a high degree of fine-tuning in order to account for the current value of dark energy parameter  $\Omega_{0,\text{DE}} \sim 0.7$ .

The following point deserves mention in a discussion of DE sourced by an oscillating scalar field. It has been noted that such models are prone to developing a dynamical instability [30]. Therefore, in order to remain viable, the scalar field in these models must begin oscillating at late times,  $z_{\text{osc}} < 5$ . This ensures that the field oscillates only a few times

<sup>7</sup>Note that this potential also plays an important role in monodromy inflation [31].

<sup>8</sup>DE in the context of  $\alpha$ -attractors has also been investigated in [32, 33]. In [33]  $\alpha$ -attractors were used to construct a model of Quintessential-Inflation, while Quintessential-Inflation in the context of oscillating DE has been discussed in [34, 35].

before the present epoch thereby limiting the growth of the instability [36]. However, the extreme case when oscillations commence very late,  $z_{\text{osc}} < 1$ , leads to a situation in which the phase of oscillations begins to play an important role and the time-averaged formula (5.2) is no longer valid [36]. Taking account of these different factors, we have chosen, for  $n = 0.05$ ,  $V_0 \sim 5 \times 10^{-47} \text{ GeV}^4$ , thereby ensuring that oscillations commence by  $z_{\text{osc}} \sim 2$ . Our results, summarized in figure 18 demonstrate that the (fine-tuned) initial value  $\rho_\varphi$  which results in  $\Omega_{0,\text{DE}} = 0.69$ , is given by

$$\rho_A = 4.51 \times 10^{-47} \text{ GeV}^4 . \quad (5.3)$$

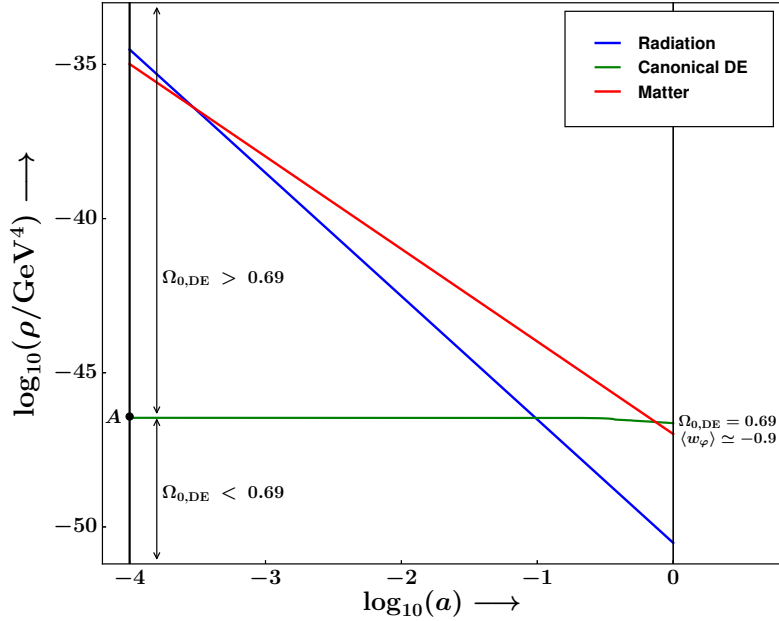


**Figure 18:** This figure describes the fine tuning of the initial scalar-field energy density associated with dark energy. Commencing our integration at  $a = 10^{-4}$  ( $z = 10^4$ ), we find that the scalar-field energy density remains frozen to its initial value all the way until  $z \sim 2$ . Thereafter, due to the rapid decline in the matter density, the damping on the scalar field gets lifted and  $\varphi$  begins to oscillate and behave like dark energy with  $\langle w_\varphi \rangle \simeq -0.9$ . The initial scalar-field energy density which results in  $\Omega_{0,\text{DE}} \simeq 0.69$  is shown by the point A. Initial values of  $\rho_i < \rho_A$  lead to too little dark energy at the present epoch ( $\Omega_{0,\text{DE}} < 0.69$ ), whereas  $\rho_i > \rho_A$  leads to too much dark energy ( $\Omega_{0,\text{DE}} > 0.69$ ).

We therefore find that the canonical potential (5.1) suffers from a severe fine-tuning problem since, for a given value of  $n$  and  $V_0$ , there is only a very narrow range of values<sup>9</sup> of the initial energy density which lead to the current value of dark energy density  $\Omega_{0,\text{DE}}$ . This is very similar to the fine tuning which afflicts dark matter with the  $m^2\varphi^2$  potential, discussed in section 4.1.

<sup>9</sup>Note that, as in the case of canonical dark matter in section 4.1, the fine tuning which we observe is insensitive to the initial value of  $\dot{\varphi}$ .

Next, we determine the effect of varying  $V_0$  on the initial field value  $\varphi_i$ . Figure 19 illustrates the relationship between  $\varphi_i$  and  $V_0$  for two different cases: (i)  $n = 0.05 \Rightarrow \langle w_\varphi \rangle \simeq -0.9$ , (ii)  $n = 0.1 \Rightarrow \langle w_\varphi \rangle \simeq -0.82$ . We observe that larger values of  $\Omega_{0,\text{DE}}$  requires a larger  $\varphi_i$  for a given  $V_0$ . (Note that  $\dot{\varphi} \simeq 0$  initially, since the motion of the dark-energy field is heavily damped, initially by radiation and then by matter. As a result,  $\rho_i \simeq V_0 |\varphi_i/m_p|^{2n}$ .)

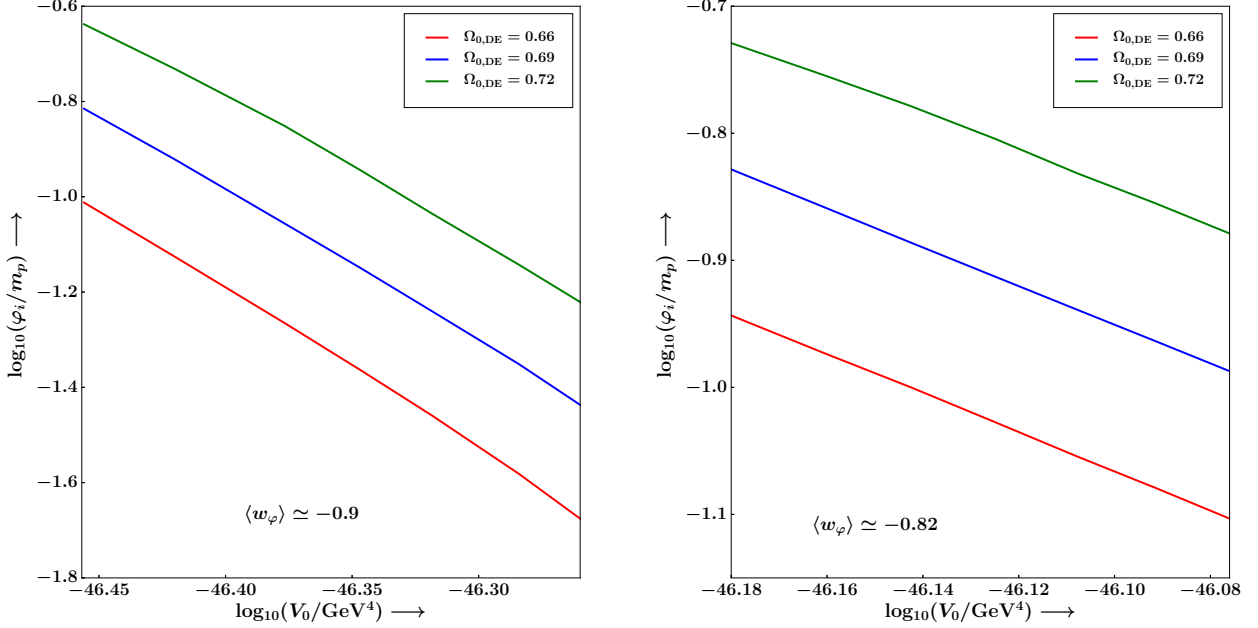


**Figure 19:** Dependence of the initial value of the scalar field  $\varphi_i$  on  $V_0$  is shown for the canonical dark-energy potential  $V(\varphi) = V_0 |\varphi/m_p|^{2n}$ . The left panel (a) and the right panel (b) correspond to  $n = 0.05$  and  $0.1$ , respectively. Three different values of the present dark energy density  $\Omega_{0,\text{DE}}$  are assumed. One sees that, for a given value of  $\Omega_{0,\text{DE}}$ , the value of  $\varphi_i$  decreases with increasing  $V_0$ . Whereas for a fixed value of  $V_0$ , larger values of  $\Omega_{0,\text{DE}}$  are associated with larger initial values of  $\varphi_i$ .

## 5.2 Dark Energy from the asymmetric *E-Model*

As we saw earlier, the *E-model* has features common to both the T-model and tracker DE. We shall therefore confine our attention solely to this model in our investigation of DE from  $\alpha$ -attractors since its properties will carry over to the other two models as well. The potential

$$V(\varphi) = V_0 \left(1 - e^{-\lambda \frac{\varphi}{m_p}}\right)^{2n}, \quad n < \frac{1}{2}, \quad (5.4)$$

exhibits three asymptotic regions given by (see figure 20)

$$\text{tracker wing: } V(\varphi) \simeq V_0 e^{2n\lambda|\varphi|/m_p}, \quad \varphi < 0, \quad \lambda|\varphi| \gg m_p, \quad (5.5)$$

$$\text{flat wing: } V(\varphi) \simeq V_0, \quad \lambda\varphi \gg m_p, \quad (5.6)$$

$$\text{oscillatory region: } V(\varphi) \simeq V_0 \left|\frac{\varphi}{m_p}\right|^{2n}, \quad \lambda|\varphi| \ll m_p. \quad (5.7)$$

The relation between  $\lambda$  and  $\alpha$  is given in (4.14). We focus first on the tracker wing of the potential, for which

$$\frac{\rho_\varphi}{\rho_{\text{total}}} = \frac{1}{n^2 \lambda^2} \quad \text{during radiation domination,} \quad (5.8)$$

$$\frac{\rho_\varphi}{\rho_{\text{total}}} = \frac{3}{4n^2 \lambda^2} \quad \text{during matter domination.} \quad (5.9)$$

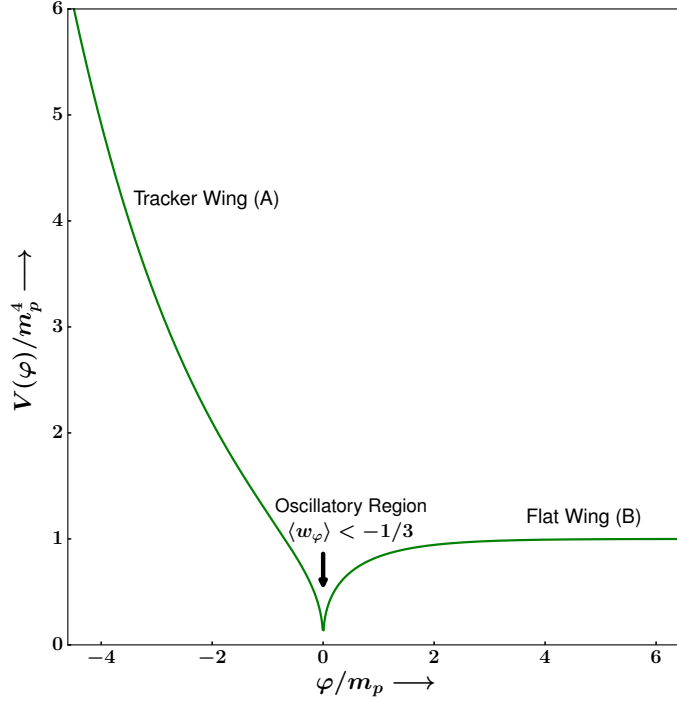


**Figure 20:** This figure schematically illustrates the *E-model* potential (5.4) with  $\lambda = 1$  and  $n = 0.2$ . The main features of this potential are: (A) the exponential tracker wing for  $\lambda|\varphi| \gg m_p$  ( $\varphi < 0$ ), (B) the flat wing for  $\lambda\varphi \gg m_p$ , and the oscillatory region for which  $\lambda|\varphi| \ll m_p$ , so that  $V(\varphi) \simeq V_0 |\varphi/m_p|^{2n}$ .

As discussed earlier, in order to evade the instabilities plaguing a cuspy potential such as (5.7), the field must commence oscillating late, by  $z_{\text{osc}} < 5$ . Choosing  $n = 0.05 \Rightarrow \langle w_\varphi \rangle \simeq -0.9$ , the values of  $V_0$  and  $\lambda$  which satisfy this constraint and which also yield  $\Omega_{0,\text{DE}} = 0.69$  are  $V_0 = 2.56 \times 10^{-47} \text{ GeV}^4$ ,  $\lambda = 60$  (hence  $\alpha = 1.85 \times 10^{-4}$ ). As in the case of  $\alpha\text{DM}$ , we find that DE based on the *E-model* converges to the late-time attractor  $V(\varphi) \sim \varphi^{2n}$  from a wide range of initial conditions. This is illustrated in figure 21. Commencing at  $a = 10^{-4}$  ( $z \sim 10^4$ ), we find that initial energy-density values spanning almost 4 orders of magnitude converges to the attractor curve (green line) yielding  $\Omega_{0,\text{DE}} = 0.69$ ; see the right panel of figure 21.

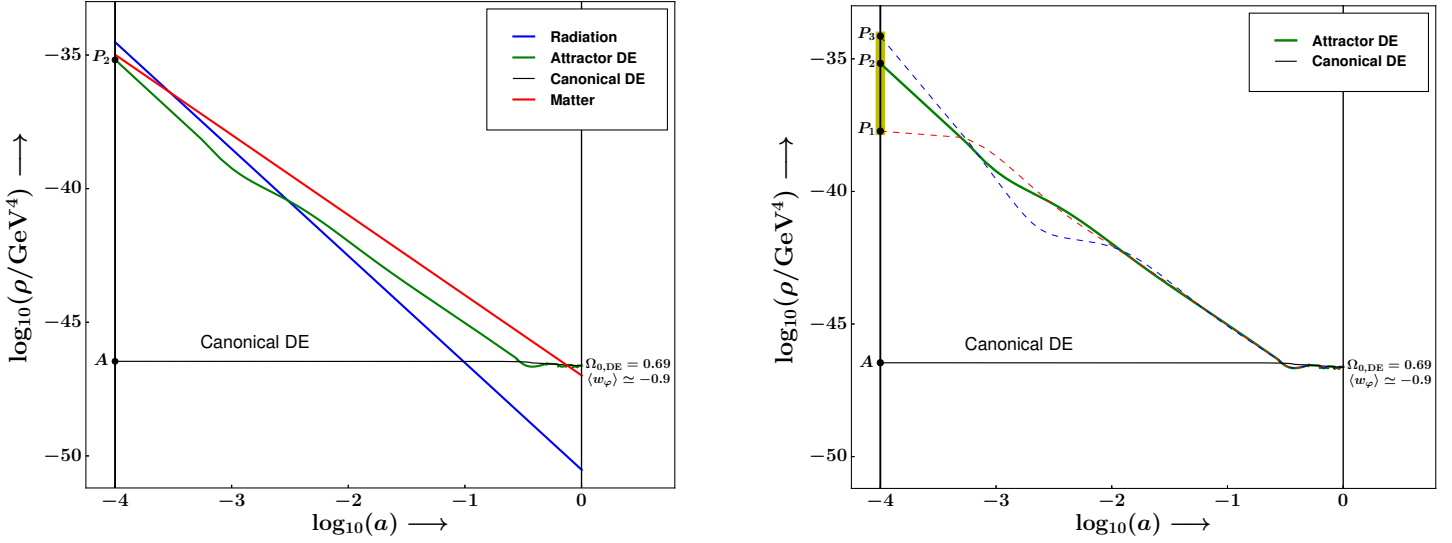


**Figure 21:** This figure describes the evolution of the energy density in radiation, matter and a scalar field, with the latter playing the role of DE. The scalar field commences its descent from the tracker wing of the potential  $V(\varphi) = V_0 (1 - e^{-\lambda\varphi/m_p})^{2n}$  with  $n = 0.05$ ,  $\lambda = 60$  and  $V_0 = 2.56 \times 10^{-47} \text{ GeV}^4$ . These parameter values ensure  $\langle w_\varphi \rangle \simeq -0.9$  and  $\Omega_{0,\text{DE}} = 0.69$ . *Left panel (a):* The green line represents DE which tracks the radiation and matter energy densities during the radiative and matter-dominated epochs, respectively. The near-horizontal black line corresponds to canonical DE (5.1) whose fine-tuned initial value is represented by point A. *Right panel:* The green band spanning from  $P_1$  to  $P_3$  shows the range in initial values of the scalar-field density (at  $z = 10^4$ ) that lead to the current value  $\Omega_{0,\text{DE}} = 0.69$ .  $P_2$  marks the initial density corresponding to the attractor solution (green line) towards which all trajectories commencing from the  $P_1$ – $P_3$  band converge. This scenario is in sharp contrast to the case of the canonical model with  $V(\varphi) = V_0 |\varphi/m_p|^{2n}$ , shown in figure 18, for which only finely tuned initial values of the energy density (point A), lead to  $\Omega_{0,\text{DE}} \simeq 0.69$ . (For clarity of presentation, we do not show the baryon density in either panel.)

The attractor value of the initial density (marked by point  $P_2$  in figure 21) is given by  $\rho_{P_2} = 6.82 \times 10^{-36} \text{ GeV}^4$ , while the maximum and minimum values of the initial density which yield  $\Omega_{0,\text{DE}} = 0.69$  are

$$\rho_{\text{max}} = \rho_{P_3} = 3.98 \times 10^{-35} \text{ GeV}^4, \quad (5.10)$$

$$\rho_{\text{min}} = \rho_{P_1} = 1.59 \times 10^{-38} \text{ GeV}^4. \quad (5.11)$$

The range in the attractor  $P_1$ – $P_3$  band will clearly increase if we commence evolving our system of equations from a more realistic earlier epoch. For instance, the range in the energy-density values prescribed at the GUT scale ( $z \sim 10^{26}$ ) which converges to  $\Omega_{0,\text{DE}} = 0.69$  covers more than 112 orders of magnitude. The fact that such an impressively large range of initial conditions can lead to the present universe removes the extreme fine-tuning associated with the potential (5.1) and makes DE from tracker potentials more compelling.

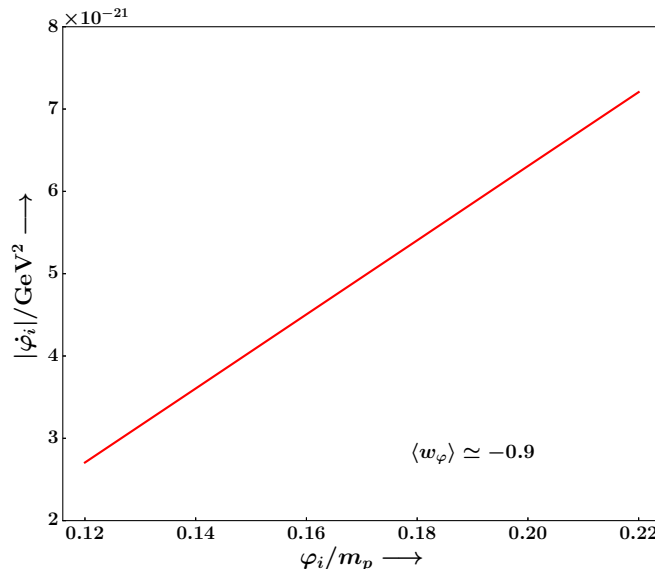


**Figure 22:** The initial velocity  $\dot{\varphi}_i$  which results in  $\Omega_{0,\text{DE}} = 0.69$  is plotted as a function of  $\varphi_i$  for the flat wing of the asymmetric *E-model* potential (5.4). The parameter values are  $V_0 = 2.56 \times 10^{-47} \text{ GeV}^4$ ,  $\lambda = 60$  and  $n = 0.05 \Rightarrow \langle w_\varphi \rangle \simeq -0.9$ . Notice that a larger initial value of the scalar field  $\varphi_i$  requires a larger value of  $|\dot{\varphi}_i|$  to ensure  $\Omega_{0,\text{DE}} = 0.69$ .

Turning to the flat right wing of the potential (5.4), one notices that the initial velocity  $\dot{\varphi}_i$  plays an important role in the analysis of initial conditions just as it did for dark matter (see section 4.2.2). Commencing on the flat wing, a given initial value  $\varphi_i$  requires a particular value of  $\dot{\varphi}_i$  in order to give rise to  $\Omega_{0,\text{DE}} = 0.69$ . The dependence of the initial velocity  $\dot{\varphi}_i$  on  $\varphi_i$  is shown in figure 22. This figure shows that that a larger  $\varphi_i$ , associated with a point further along the flat wing, requires a larger value of  $|\dot{\varphi}_i|$  in order to arrive at a given  $\Omega_{0,\text{DE}}$  (also see figure 11).

We therefore conclude that, from the viewpoint of initial conditions, the flat wing of the *E-model* potential results in a less appealing model of DE as compared to the steep wing, for which one arrives at a given  $\Omega_{0,\text{DE}}$  from a much wider class of initial conditions.

## 6 Discussion

In this paper, we have demonstrated that the  $\alpha$ -attractors, which provide interesting models of inflation [1, 2], can also lead to compelling models of dark matter and perhaps even dark energy. It is well known that a simple scalar field model of dark matter can be constructed from the potential usually associated with chaotic inflation, namely  $V = \frac{1}{2}m^2\varphi^2$ . For an ultra-light mass of  $m \sim 10^{-22} \text{ eV}$ , this model can successfully resolve several key problems faced by the standard cold dark matter scenario including the cusp-core issue, the problem of substructure etc. [8, 15, 18]. However, what is sometimes overlooked is that this interesting model also suffers from a severe fine-tuning issue. As demonstrated in section 4.1, for a given value of  $m$ , the region of initial values of  $\varphi_i$  which leads to the current value of the matter density  $\Omega_{0m}$  is exceedingly small. Moreover the fine tuning discussed here is expected to carry over to other potentials with an  $m^2\varphi^2$  asymptote including axionic dark matter.



This difficulty is avoided if dark matter is sourced by  $\alpha$ -attractors. Of the  $\alpha$ -attractor models studied in sec. 4, the *E-model* (3.4) and the tracker potential (3.5) provide the most versatile examples of scalar-field dark matter. In both, one arrives at the late-time dark matter asymptote from a very wide range of initial conditions. An important feature of the asymmetric *E-model* is the presence of a steep non-inflationary wing of the potential in addition to the inflationary plateau, as shown in figure 4. The required steepness of the tracker wing is supported by a small value of the geometric parameter  $\alpha \leq 10^{-3}$ . This is the main difference with the Starobinsky model  $R + M^2 R^2$ , which corresponds to  $\alpha = 1$ . An analogous requirement is valid for the tracker potential (3.5). These two  $\alpha$ -attractor models, therefore, successfully overcome the fine-tuning problems associated with the  $m^2\varphi^2$  potential.

Another important feature of  $\alpha$ -dark matter, shared by the  $m^2\varphi^2$  potential, is that the Jeans length associated with gravitational clustering can be quite large. Our analysis in section 4.5 demonstrates that, despite significant differences in dynamics, the Jeans scale in all of our DM models converges to the same late-time expression (4.27). We therefore conclude that *tracker based*  $\alpha$ -dark matter shares all of the distinctive features of *fuzzy* dark matter (sourced by the  $m^2\varphi^2$  potential), without having any of its limitations.

Finally, we would like to caution the reader that our attempt in this paper has not been to create a unified description of inflation and dark matter based on  $\alpha$ -attractors. It has been more modest. We have simply shown that the very same potentials which characterize  $\alpha$ -attractors can also be used to construct compelling models of dark matter, and perhaps even dark energy. Nevertheless, one can, in principle, envisage the possibility that dark matter arose from the coherent oscillations in the  $\alpha$ -attractor inflaton after reheating. This follows from the observation that all of the  $\alpha$ -attractor potentials have a minimum near which  $V \simeq \frac{1}{2}m^2\varphi^2$ , which permits the inflaton to oscillate. In the standard scenario, the universe preheats during this oscillatory phase due to the coupling of  $\varphi$  to the standard model fields. Preheating transfers the energy of the inflaton into new degrees of freedom (quarks and leptons, radiation etc.) created during preheating. Consequently, the value of the inflaton drops drastically from  $\varphi \sim m_p$  at the commencement of preheating to  $\varphi_{\text{end}} \ll m_p$  at its end. If  $\varphi_{\text{end}} \neq 0$  (i.e., if preheating is not complete), then the post-preheating oscillations of  $\varphi$  will cause the inflaton density to drop as  $\rho_\varphi \propto a^{-3}$  a consequence of the fact that  $\langle w_\varphi \rangle \simeq 0$ . In other words, the inflaton can now play the role of dark matter [37, 38]. It is straightforward to show that if the universe preheats to a temperature  $T_r$  then, at  $z_r = T_r/T_0 - 1$ , the dark-matter field must satisfy the relation

$$\frac{1}{2}m^2\varphi_r^2 \simeq \rho_r(z_r) \frac{T_{0\gamma}}{T_\gamma(z_r)} \frac{\Omega_{0m}}{\Omega_{0r}}, \quad (6.1)$$

where  $\varphi_r \equiv \varphi(z_r)$  and  $\rho_r = \sigma T_r^4$  is the radiation density immediately after preheating. In other words

$$\varphi_r \simeq \left[ \frac{2\rho_r(z_r)}{m^2} \frac{T_{0\gamma}}{T_\gamma(z_r)} \frac{\Omega_{0m}}{\Omega_{0r}} \right]^{1/2}. \quad (6.2)$$

Post-preheating scalar field values  $\varphi > \varphi_r$  will lead to an excess of dark matter, whereas  $\varphi < \varphi_r$  will result in too little dark matter at the current epoch. A similar fine tuning of initial conditions for the  $m^2\varphi^2$  potential was noted earlier in section 4.1.

The reader might also note that our attempt in this paper has been to investigate the many different features associated with  $\alpha$ DM and  $\alpha$ DE. We have intentionally refrained from testing these models against observations, leaving this exercise to a future paper.

## Acknowledgments

S.S.M. thanks the Council of Scientific and Industrial Research (CSIR), India, for financial support as senior research fellow.

## A Linear perturbations and instability

The Friedmann–Robertson–Walker metric with scalar perturbations has the form

$$ds^2 = (1 + 2\Psi)dt^2 - a^2(t)(1 - 2\Psi)d\vec{x}^2. \quad (\text{A.1})$$

The linearized equations for perturbations read

$$\delta\ddot{\varphi} + 3H\delta\dot{\varphi} + V''(\varphi)\delta\varphi - \frac{\nabla^2}{a^2}\delta\varphi = 4\dot{\varphi}\dot{\Psi} - 2V'(\varphi)\Psi, \quad (\text{A.2})$$

$$\frac{\nabla^2}{a^2}\Psi = \frac{1}{2m_p^2} [\dot{\varphi}\delta\dot{\varphi} + V'(\varphi)\delta\varphi + 3H\dot{\varphi}\delta\varphi - \dot{\varphi}^2\Psi], \quad (\text{A.3})$$

where an overdot denotes the derivative with respect to the time  $t$ . Here, we use the background equations

$$H^2 = \frac{\rho}{3m_p^2} = \frac{1}{3m_p^2} \left[ \frac{1}{2}\dot{\varphi}^2 + V(\varphi) \right], \quad \dot{H} = -\frac{(\rho + p)}{2m_p^2} = -\frac{\dot{\varphi}^2}{2m_p^2}, \quad (\text{A.4})$$

and

$$\ddot{\varphi} + 3H\dot{\varphi} + V'(\varphi) = 0, \quad (\text{A.5})$$

with  $H = \dot{a}/a$ . All equations are also valid if the potential  $V(\varphi)$  includes the cosmological constant.

In the domain of interest,

$$H^2, |\dot{H}| \ll \frac{k^2}{a^2} \ll m^2, \quad (\text{A.6})$$

where  $m$  is the mass of the scalar field, several terms in the system of equations (A.2), (A.3) can be neglected so that this system simplifies to

$$\delta\ddot{\varphi} + V''(\varphi)\delta\varphi - \frac{\nabla^2}{a^2}\delta\varphi \approx 4\dot{\varphi}\dot{\Psi} - 2V'(\varphi)\Psi, \quad (\text{A.7})$$

$$\frac{\nabla^2}{a^2}\Psi \approx \frac{1}{2m_p^2} [\dot{\varphi}\delta\dot{\varphi} + V'(\varphi)\delta\varphi]. \quad (\text{A.8})$$

Proceeding to the Fourier transform and systematically using (A.6), we have from (A.8):

$$\Psi \approx -\frac{a^2}{2m_p^2 k^2} [\dot{\varphi}\delta\dot{\varphi} + V'(\varphi)\delta\varphi], \quad \dot{\Psi} \approx -\frac{a^2\dot{\varphi}}{2m_p^2 k^2} [\delta\ddot{\varphi} + V''(\varphi)\delta\varphi]. \quad (\text{A.9})$$

Substituting this into (A.7), we obtain a closed approximate equation for  $\delta\varphi$ :

$$\delta\ddot{\varphi} + V''(\varphi)\delta\varphi + \frac{k^2}{a^2}\delta\varphi - \frac{a^2 V'(\varphi)}{m_p^2 k^2} [\dot{\varphi}\delta\dot{\varphi} + V'(\varphi)\delta\varphi] = 0. \quad (\text{A.10})$$

One can see that the approximation (A.6) practically means that we can neglect the cosmological expansion altogether for the wavenumbers  $k$  of interest and also that we use formal perturbation theory to the leading order of the gravitational coupling  $1/m_p^2$ . The change of variables

$$\delta\varphi = \left[1 + \frac{a^2 V(\varphi)}{2m_p^2 k^2}\right] v \quad (\text{A.11})$$

in (A.10) eliminates, in the same approximation, the term with the first derivative for  $v$ , and we obtain

$$\ddot{v} + \left[ V'' + \frac{k^2}{a^2} - \frac{a^2}{2m_p^2 k^2} (3V'^2 - V''\dot{\varphi}^2) \right] v = 0. \quad (\text{A.12})$$

In connection with our approximation, we set  $a = 1$  and investigate this equation for different potentials  $V(\varphi)$ .

- In the simplest case

$$V(\varphi) = \frac{1}{2} m^2 \varphi^2, \quad (\text{A.13})$$

the scalar field oscillates as  $\varphi = \varphi_0 \cos mt$ , and we get the equation

$$\ddot{v} + \left( m^2 + k^2 - \frac{m^4 \varphi_0^2}{2m_p^2 k^2} - \frac{m^4 \varphi_0^2}{m_p^2 k^2} \cos 2mt \right) v = 0. \quad (\text{A.14})$$

By proceeding to the dimensionless time variable  $\tau = mt$ , we transform this into the canonical Mathieu equation

$$\ddot{v} + (P - 2Q \cos 2\tau) v = 0 \quad (\text{A.15})$$

with

$$P = 1 + \frac{k^2}{m^2} - \frac{m^2 \varphi_0^2}{2m_p^2 k^2}, \quad Q = \frac{m^2 \varphi_0^2}{2m_p^2 k^2}. \quad (\text{A.16})$$

Our domain of values of  $k$  ensures that the value of  $P$  lies very close to unity. In this case, the instability domain for the Mathieu equation corresponds to

$$|Q| > |P - 1|. \quad (\text{A.17})$$

We obtain the condition which coincides with the result of [15]:

$$k^4 < \frac{m^4 \varphi_0^2}{m_p^2} = \frac{2m^2 \rho_\varphi}{m_p^2}. \quad (\text{A.18})$$

- In the case

$$V(\varphi) = \frac{1}{2} m^2 \varphi^2 + \frac{1}{4} \lambda_0 \varphi^4 \quad (\text{A.19})$$

with the additional condition  $\lambda_0 \varphi^2 \ll m^2$ , we can include the corresponding correction to the leading part in (A.12), that survives in the limit  $m_p \rightarrow \infty$ . This results in the

same Mathieu equation (A.15) with  $P$  and  $Q$  shifted with respect to the preceding case as  $P \rightarrow P + 3\lambda_0\varphi_0^2/2m^2$ ,  $Q \rightarrow Q - 3\lambda_0\varphi_0^2/4m^2$ . Condition (A.17) then reads

$$k^4 + \frac{9}{4}\lambda_0\varphi_0^2k^2 < \frac{m^4\varphi_0^2}{m_p^2}, \quad (\text{A.20})$$

which, apart from the coefficient of the second term on the left-hand side, essentially coincides with the result of [30].

- Finally, consider the case with a cubic term in the potential, i.e.,

$$V(\varphi) = \frac{1}{2}m^2\varphi^2 - \frac{1}{3}\mu\varphi^3 + \frac{1}{4}\lambda_0\varphi^4 \quad (\text{A.21})$$

with the condition  $\lambda_0\varphi_0^2, \mu\varphi \ll m^2$ . In this case, the main equation (A.12) reads

$$\ddot{v} + \left[ m^2 + k^2 + \frac{3}{2}\lambda_0\varphi_0^2 - \frac{m^4\varphi_0^2}{2m_p^2k^2} + 2\mu\varphi_0 \cos mt + \left( \frac{3}{2}\lambda_0\varphi_0^2 - \frac{m^4\varphi_0^2}{m_p^2k^2} \right) \cos 2mt \right] v = 0 \quad (\text{A.22})$$

There appears a term in (A.22) which oscillates with frequency  $m$ . The resonance instability in the corresponding lowest-frequency zone centered at frequency  $\omega = m/2$  in this case requires the condition

$$\frac{\mu\varphi_0}{m^2} > \frac{3}{4} + \frac{k^2}{m^2} - \frac{m^2\varphi_0^2}{2m_p^2k^2}, \quad (\text{A.23})$$

which is incompatible with our assumptions  $\mu\varphi_0 \ll m^2$  and  $H^2 = m^2\varphi_0^2/3m_p^2 \ll k^2 \ll m^2$ . However, in the next instability zone centered at frequency  $\omega = m$ , there arises a second-order resonance caused by the term  $2\mu\varphi_0 \cos mt$  in (A.22). Combined with the first-order resonance for the quartic term, the resulting resonance condition reads

$$k^4 + \left[ \frac{9}{4}\lambda_0\varphi_0^2 - \frac{5}{3} \left( \frac{\mu\varphi_0}{m} \right)^2 \right] k^2 \lesssim \frac{m^4\varphi_0^2}{m_p^2}, \quad (\text{A.24})$$

and represents a generalization of (A.20). The details of derivation of this expression are presented in the next section.

## B Parametric resonance to second order

In this section, we provide an analysis of the parametric resonance in (A.22) to second order of perturbation theory and, in particular, justify the expression (A.24).

Consider a general equation of the form (A.22) for a variable  $Y$ :

$$\ddot{Y} + [\omega_0^2 - \epsilon(2Q_1 \cos \omega t + 2Q_2 \cos 2\omega t)] Y = 0, \quad (\text{B.1})$$

where  $\omega_0$ ,  $\omega$ ,  $Q_1$  and  $Q_2$  are constant in time, and  $\epsilon$  is an explicit small parameter introduced for considerations of perturbation theory, which indicates the smallness of  $Q_1$  and  $Q_2$  relative to  $\omega^2$ , and which at the end of calculations can be set to unity. We will be looking for the regions of instability with respect to the variable proper frequency  $\omega_0$  order by order in perturbation theory in  $\epsilon$ . It is well known (or can be verified by the theory developed below) that the resonance zones for equation (B.1) are located around the frequencies  $\omega_0 = s\omega/2$

with  $s = 1, 2, \dots$ . For this reason, for every natural  $s$ , we introduce the quantity  $\Delta_s$  defined as

$$\epsilon \Delta_s = \left( \frac{s\omega}{2} \right)^2 - \omega_0^2. \quad (\text{B.2})$$

Equation (B.1) then becomes

$$\ddot{Y} + \left( \frac{s\omega}{2} \right)^2 Y = \epsilon (2Q_1 \cos \omega t + 2Q_2 \cos 2\omega t + \Delta_s) Y. \quad (\text{B.3})$$

The general asymptotic method developed in [39] consists in looking for solutions to (B.3) in the form of expansion in powers of  $\epsilon$ :

$$Y = a \cos \frac{s\omega t}{2} + b \sin \frac{s\omega t}{2} + \epsilon u^{(1)} + \epsilon^2 u^{(2)} + \dots, \quad (\text{B.4})$$

where  $a$  and  $b$  are slowly varying functions of time, obeying the system of equations

$$\begin{aligned} \dot{a} &= \epsilon A^{(1)}(a, b) + \epsilon^2 A^{(2)}(a, b) + \dots, \\ \dot{b} &= \epsilon B^{(1)}(a, b) + \epsilon^2 B^{(2)}(a, b) + \dots, \end{aligned} \quad (\text{B.5})$$

and  $u^{(k)}$ ,  $k = 1, 2, \dots$ , are functions of  $a$ ,  $b$  and  $t$ , periodic in the last argument with period  $4\pi/\omega$ :

$$u^{(k)}(a, b, t) = \sum_{n \in \mathbb{Z}} u_n^{(k)}(a, b) e^{in\omega t/2}. \quad (\text{B.6})$$

The method consists in looking for the functions  $A^{(k)}(a, b)$ ,  $B^{(k)}(a, b)$  and  $u_n^{(k)}(a, b)$ . Equations (B.5) then will indicate the domains of instability with respect to the growth of amplitudes  $a$  and  $b$ .

For our purposes, it will be necessary to develop the theory to second order in  $\epsilon$ . Differentiating (B.4) and using (B.5), we find

$$\begin{aligned} \dot{Y} &= \frac{s\omega}{2} \left( -a \sin \frac{s\omega t}{2} + b \cos \frac{s\omega t}{2} \right) + \left( \epsilon A^{(1)} + \epsilon^2 A^{(2)} \right) \cos \frac{s\omega t}{2} + \left( \epsilon B^{(1)} + \epsilon^2 B^{(2)} \right) \sin \frac{s\omega t}{2} \\ &\quad + \epsilon \dot{u}^{(1)} + \epsilon^2 \dot{u}^{(2)} + \epsilon^2 \left( u_a^{(1)} A^{(1)} + u_b^{(1)} B^{(1)} \right) + o(\epsilon^2), \end{aligned} \quad (\text{B.7})$$

$$\begin{aligned} \ddot{Y} &= - \left( \frac{s\omega}{2} \right)^2 \left( a \cos \frac{s\omega t}{2} + b \sin \frac{s\omega t}{2} \right) \\ &\quad - \left( \epsilon A^{(1)} + \epsilon^2 A^{(2)} \right) s\omega \sin \frac{s\omega t}{2} + \left( \epsilon B^{(1)} + \epsilon^2 B^{(2)} \right) s\omega \cos \frac{s\omega t}{2} \\ &\quad + \epsilon^2 \left( A_a^{(1)} A^{(1)} + A_b^{(1)} B^{(1)} \right) \cos \frac{s\omega t}{2} + \epsilon^2 \left( B_a^{(1)} A^{(1)} + B_b^{(1)} B^{(1)} \right) \sin \frac{s\omega t}{2} \\ &\quad + \epsilon \ddot{u}^{(1)} + \epsilon^2 \ddot{u}^{(2)} + 2\epsilon^2 \left( \dot{u}_a^{(1)} A^{(1)} + \dot{u}_b^{(1)} B^{(1)} \right) + o(\epsilon^2), \end{aligned} \quad (\text{B.8})$$

where the subscripts ‘ $a$ ’ and ‘ $b$ ’ denote partial derivatives with respect to these variables, and the dots over  $u^{(k)}$  denote partial derivatives with respect to its last (time) argument.

We substitute (B.4) and (B.8) into (B.3) and collect terms with respective order in  $\epsilon$ . The zero-order equation is satisfied automatically. In the first order in  $\epsilon$ , we obtain

$$\begin{aligned}\ddot{u}^{(1)} + \left(\frac{s\omega}{2}\right)^2 u^{(1)} &= \sum_n \left[ \left(\frac{s\omega}{2}\right)^2 - \left(\frac{n\omega}{2}\right)^2 \right] u_n^{(1)} e^{in\omega t/2} \\ &= (2Q_1 \cos \omega t + 2Q_2 \cos 2\omega t + \Delta_s) \left( a \cos \frac{s\omega t}{2} + b \sin \frac{s\omega t}{2} \right) \\ &\quad + A^{(1)} s\omega \sin \frac{s\omega t}{2} - B^{(1)} s\omega \cos \frac{s\omega t}{2}.\end{aligned}\quad (\text{B.9})$$

The terms with  $n = \pm s$  on the left-hand side vanish. Therefore, the corresponding terms in the Fourier expansion of the right-hand side should vanish as well. This leads to the condition of zero  $A^{(1)}$  and  $B^{(1)}$  unless  $s = 1$  or  $s = 2$ . Thus, there are two potential resonance zones in the first order in  $\epsilon$ . We get the following expressions in these zones:

$$A^{(1)} = \frac{Q_s - \Delta_s}{s\omega} b, \quad B^{(1)} = \frac{Q_s + \Delta_s}{s\omega} a, \quad s = 1, 2. \quad (\text{B.10})$$

In the first order in  $\epsilon$ , the two resonant terms in (B.3) with amplitudes  $Q_1$  and  $Q_2$  act independently each in its own resonance zone.

We should also determine the nonzero coefficients  $u_n^{(1)}$ . Note that the components with  $n = \pm s$  remain undetermined, but they can be set to zero because the oscillatory terms with these frequencies are already present as the first two terms in (B.4). For the nonzero terms, from (B.9), we get

$$u_3^{(1)} = -\frac{1}{4\omega^2} \left[ (Q_1 + Q_2) a - i(Q_1 - Q_2) b \right], \quad u_5^{(1)} = \frac{i}{12\omega^2} Q_2 b, \quad s = 1, \quad (\text{B.11})$$

$$u_0^{(1)} = \frac{Q_1}{\omega^2} a, \quad u_4^{(1)} = -\frac{Q_1}{6\omega^2} (a - ib), \quad u_6^{(1)} = -\frac{Q_2}{16\omega^2} (a - ib), \quad s = 2, \quad (\text{B.12})$$

and  $u_{-q}^{(1)} = \bar{u}_q^{(1)}$  due to the reality of  $u^{(1)}$ .

In the second order in  $\epsilon$ , we get the equation

$$\begin{aligned}\ddot{u}^{(2)} + \left(\frac{s\omega}{2}\right)^2 u^{(2)} &= (2Q_1 \cos \omega t + 2Q_2 \cos 2\omega t + \Delta_s) u^{(1)} \\ &\quad + A^{(2)} s\omega \sin \frac{s\omega t}{2} - B^{(2)} s\omega \cos \frac{s\omega t}{2} \\ &\quad - \left( A_a^{(1)} A^{(1)} + A_b^{(1)} B^{(1)} \right) \cos \frac{s\omega t}{2} - \left( B_a^{(1)} A^{(1)} + B_b^{(1)} B^{(1)} \right) \sin \frac{s\omega t}{2} \\ &\quad - 2 \left( \dot{u}_a^{(1)} A^{(1)} + \dot{u}_b^{(1)} B^{(1)} \right).\end{aligned}\quad (\text{B.13})$$

Expanding both sides in Fourier series, and taking into account (B.10) with an implication  $A_a^{(1)} = B_b^{(1)} = 0$ , we obtain

$$\begin{aligned}\sum_n \left[ \left(\frac{s\omega}{2}\right)^2 - \left(\frac{n\omega}{2}\right)^2 \right] u_n^{(2)} e^{in\omega t/2} &= (2Q_1 \cos \omega t + 2Q_2 \cos 2\omega t + \Delta_s) \sum_p u_p^{(1)} e^{ip\omega t/2} \\ &\quad + A^{(2)} s\omega \sin \frac{s\omega t}{2} - B^{(2)} s\omega \cos \frac{s\omega t}{2} \\ &\quad - A_b^{(1)} B^{(1)} \cos \frac{s\omega t}{2} - B_a^{(1)} A^{(1)} \sin \frac{s\omega t}{2} \\ &\quad - i\omega \sum_p \left( u_{p,a}^{(1)} A^{(1)} + u_{p,b}^{(1)} B^{(1)} \right) p e^{ip\omega t/2}.\end{aligned}\quad (\text{B.14})$$

We are interested only in the lowest two resonance zones with  $s = 1$  and  $s = 2$ . Again, the terms with  $n = \pm s$  on the left-hand side of the last equation vanish. Therefore, the corresponding terms in the Fourier expansion of the right-hand side should vanish as well, which condition determines the sought functions  $A^{(2)}$  and  $B^{(2)}$ . Taking into account (B.10)–(B.12), we obtain

$$A^{(2)} = \frac{b}{\omega^3} \left[ Q_1^2 - \Delta_1^2 + \frac{1}{2} (Q_1 - Q_2)^2 + \frac{1}{6} Q_2^2 \right], \quad (\text{B.15})$$

$$B^{(2)} = \frac{a}{\omega^3} \left[ \Delta_1^2 - Q_1^2 - \frac{1}{2} (Q_1 + Q_2)^2 \right], \quad s = 1, \quad (\text{B.16})$$

$$A^{(2)} = \frac{b}{8\omega^3} \left[ Q_2^2 - \Delta_2^2 + \frac{4}{3} Q_1^2 + \frac{1}{2} Q_2^2 \right], \quad (\text{B.17})$$

$$B^{(2)} = \frac{a}{8\omega^3} \left[ \Delta_2^2 - Q_2^2 + \frac{20}{3} Q_1^2 - \frac{1}{2} Q_2^2 \right], \quad s = 2. \quad (\text{B.18})$$

One can see that, in both resonance zones, up to second order in  $\epsilon$ , the evolution equations have the linear form

$$\dot{a} = Ab, \quad \dot{b} = Ba, \quad (\text{B.19})$$

so that the instability region is determined by the condition  $AB > 0$ . Setting  $\epsilon = 1$ , we obtain, for the coefficients  $A$  and  $B$  in (B.19),

$$A = \frac{Q_1 - \Delta_1}{\omega} + \frac{1}{\omega^3} \left[ Q_1^2 - \Delta_1^2 + \frac{1}{2} (Q_1 - Q_2)^2 + \frac{1}{6} Q_2^2 \right], \quad (\text{B.20})$$

$$B = \frac{Q_1 + \Delta_1}{\omega} + \frac{1}{\omega^3} \left[ \Delta_1^2 - Q_1^2 - \frac{1}{2} (Q_1 + Q_2)^2 \right], \quad s = 1, \quad (\text{B.21})$$

$$A = \frac{Q_2 - \Delta_2}{2\omega} + \frac{1}{8\omega^3} \left[ Q_2^2 - \Delta_2^2 + \frac{4}{3} Q_1^2 + \frac{1}{2} Q_2^2 \right], \quad (\text{B.22})$$

$$B = \frac{Q_2 + \Delta_2}{2\omega} + \frac{1}{8\omega^3} \left[ \Delta_2^2 - Q_2^2 + \frac{20}{3} Q_1^2 - \frac{1}{2} Q_2^2 \right], \quad s = 2. \quad (\text{B.23})$$

The boundary of the instability region  $AB > 0$  in each of the two zones is determined by the equations  $A = 0$  and  $B = 0$ . We can take into account the fact of smallness of the quantities  $Q_s/\omega^2$ . In this case, up to second order in these quantities, we have  $\Delta_s^2 - Q_s^2 = 0$ . Therefore, the roots of (B.20)–(B.23) with respect to  $\Delta_s$  to second order in  $Q_s/\omega^2$  can be given by dropping the terms  $\Delta_s^2 - Q_s^2$  from these equations. For the two zones of interest, we then have the expressions for the upper ( $\Delta_s^+$ ) and lower ( $\Delta_s^-$ ) boundary values of the instability zones, depending on the signs of  $Q_1$  and  $Q_2$ :

$$\Delta_1^\pm = \begin{cases} Q_1 + \frac{1}{2\omega^2} \left[ (Q_1 - Q_2)^2 + \frac{1}{3} Q_2^2 \right], \\ -Q_1 + \frac{1}{2\omega^2} (Q_1 + Q_2)^2, \end{cases} \quad (\text{B.24})$$

$$\Delta_2^\pm = \begin{cases} Q_2 + \frac{1}{\omega^2} \left( \frac{1}{3} Q_1^2 + \frac{1}{8} Q_2^2 \right), \\ -Q_2 - \frac{1}{\omega^2} \left( \frac{5}{3} Q_1^2 - \frac{1}{8} Q_2^2 \right). \end{cases} \quad (\text{B.25})$$

Let us apply these general results to the theory described by equation (A.22). We have, in this case,

$$\omega = m, \quad \omega_0^2 = m^2 + k^2 + \frac{3}{2}\lambda_0\varphi_0^2 - \frac{m^4\varphi_0^2}{2m_p^2k^2}, \quad (\text{B.26})$$

$$Q_1 = -\mu\varphi_0, \quad Q_2 = \left( \frac{m^4\varphi_0^2}{2m_p^2k^2} - \frac{3}{4}\lambda_0\varphi_0^2 \right), \quad (\text{B.27})$$

so that

$$\Delta_1 = -\frac{3}{4}m^2 - k^2 - \frac{3}{2}\lambda_0\varphi_0^2 + \frac{m^4\varphi_0^2}{2m_p^2k^2}, \quad (\text{B.28})$$

$$\Delta_2 = -k^2 - \frac{3}{2}\lambda_0\varphi_0^2 + \frac{m^4\varphi_0^2}{2m_p^2k^2}. \quad (\text{B.29})$$

In principle, our theory allows for the situation where  $Q_1 \gg Q_2$ . In this case, the resonance condition in the first zone would be dominated by the first-order contribution in  $Q_1$ , leading to the condition

$$\Delta_1^2 < Q_1^2. \quad (\text{B.30})$$

With the above equations (B.26)–(B.29), this translates into (A.23).

In the second resonance zone, under the same conditions, we have

$$\Delta_2^\pm \approx \begin{cases} Q_2 + \frac{1}{3\omega^2}Q_1^2, \\ -Q_2 - \frac{5}{3\omega^2}Q_1^2. \end{cases} \quad (\text{B.31})$$

For our parameters (B.26)–(B.29), the inequality  $\Delta_2^- < \Delta_2 < \Delta_2^+$  implies

$$\frac{3}{2}\lambda_0\varphi_0^2 < k^2 + \frac{9}{4}\lambda_0\varphi_0^2 + \frac{1}{3}\left(\frac{\mu\varphi_0}{m}\right)^2 < 2\left(\frac{\mu\varphi_0}{m}\right)^2 + \frac{m^2\varphi_0^2}{m_p^2k^2}. \quad (\text{B.32})$$

The lower inequality is satisfied automatically, while the upper one leads to (A.24).

## C Relationship between the mass of the scalar field and its initial value

The following conditions need to be simultaneously satisfied in order for  $\varphi$  to oscillate and play the role of dark matter: (i)  $\varphi \ll m_p$ , (ii)  $m \geq H$ .

Since the scalar field starts oscillating during the radiation dominated epoch one finds

$$m \simeq H \propto a^{-2} \Rightarrow a/a_* = \sqrt{(m_*/m)} \quad (\text{C.1})$$

$a_*$  being the epoch marking the onset of oscillations for a given mass  $m_*$ . After the scalar field commences oscillating its average equation of state becomes  $\langle \omega_\varphi \rangle = 0$  and its density falls off as  $\rho_\varphi \propto a^{-3}$ . Consequently

$$\frac{\rho}{\rho_*} = \left( \frac{a}{a_*} \right)^{-3} = \left( \frac{m}{m_*} \right)^{3/2}. \quad (\text{C.2})$$



The initial value of the density is related to the initial scalar field value by  $\rho_i = \frac{1}{2}m^2\varphi_i^2$ . Substitution in (C.2) leads to

$$\varphi_i = \varphi_{i*} \left( \frac{m}{m_*} \right)^{-1/4}. \quad (\text{C.3})$$

Finally, our numerical analysis informs us that  $\varphi_* = \frac{\sqrt{2\rho_A}}{m} = 0.06 \, m_p$  for  $m_* = 10^{-22} \, \text{eV}$ . This initial value of  $\varphi_i$  results in  $\Omega_{0m} = 0.3$ . This allows us to rewrite (C.3) as follows

$$\varphi_i = 0.06 \times \left( \frac{m}{10^{-22} \, \text{eV}} \right)^{-1/4} m_p, \quad (\text{C.4})$$

which was shown in figure 3. The corresponding relationship between  $\rho_i$  and  $m$  can easily be established using (C.4) and  $\rho_i \simeq \frac{1}{2}m^2\varphi_i^2$ .

## References

- [1] R. Kallosh and A. Linde, JCAP07 (2013) 002 [arXiv:1306.5220].
- [2] R. Kallosh, A. Linde and D. Roest, JHEP11, 198 (2013) [arXiv:1311.0472].
- [3] V. Sahni and P. Coles, Phys.Rept. **262**, 1-135 (2016) [astro-ph/9505005].
- [4] S. Dodelson, *Modern Cosmology*, Academic press, (2003).
- [5] V. Sahni, *Dark matter and dark energy*, Lect. Notes Phys. 653, 141-180 (2004) [astro-ph/0403324].
- [6] V. Sahni and A.A. Starobinsky, Int. J. Mod. Phys. **D9** 373 (2000); P. J. E. Peebles and B. Ratra, Rev. Mod. Phys. **75** 559 (2003); T. Padmanabhan, Phys. Rep. **380** 235 (2003); V. Sahni, [astro-ph/0202076], [astro-ph/0502032]; V. Sahni and A.A. Starobinsky, Int. J. Mod. Phys. **D15** 2105 (2006); E. J. Copeland, M. Sami and S. Tsujikawa, Int. J. Mod. Phys. **D15** 1753 (2006); R. Bousso, Gen. Relativ. Gravit. **40**, 607 (2008).
- [7] A.A. Starobinsky, Phys. Lett. B **91**, 99 (1980).
- [8] V. Sahni and L. Wang, Phys. Rev. D **62**, 103517 (2000) [astro-ph/9910097].
- [9] M.S. Turner, Phys. Rev. D **28**, 1243 (1983).
- [10] R. Peccei and H.R. Quinn Phys. Rev. Lett. **38**, 1440 (1977).
- [11] M. Yu. Khlopov, B.A. Malomed and Ya.B. Zeldovich, Mon. Not. Roy. Ast. Soc. **215**, 575 (1985).
- [12] S.-J. Sin, Phys. Rev. D **50**, 3650 (1994); S.U. Ji and S.-J. Sin, Phys. Rev. D **50**, 3655 (1994); J.-W. Lee and I.-G. Koh, Phys. Rev. D **53**, 2236 (1996).
- [13] P. J. E. Peebles and A. Vilenkin, Phys. Rev. D **60**, 103506 (1999); P. J. E. Peebles, Astrophys. J. **534**, L127 (2000) [astro-ph/0002495].
- [14] I. Zlatev and P.J. Steinhardt, Phys. Lett. B **459**, 570 (1999).
- [15] W.Hu, R. Barkana and A. Gruzinov, Phys. Rev. Lett. **85**, 1158 (2000).
- [16] J. Goodman, New Astronomy 5, 103 (2000).
- [17] T. Matos, F.S. Guzman and D. Nunes, Phys. Rev. D **62**, 061301 (2000); T. Matos and L. A. Ureña-López, Phys. Rev. D **63**, 063506 (2001); *A brief Review of the Scalar Field Dark Matter model*, J. Magaña, T. Matos, V. Robles, A. Suárez, [arXiv:1201.6107].
- [18] L. Hui, J. P. Ostriker, S. Tremaine and E. Witten, [arXiv:1610.08297].

- [19] F. Villaescusa and N. Dalal, JCAP 1103 (2011) 024 [arXiv:1010.3008]; M. Viel, G.D. Becker, J.S. Bolton and M.G. Haehnelt, Phys. Rev. D **88**, 043502 (2013) [arXiv:1306.2314].
- [20] V. Sahni and A.A. Sen, Eur.Phys.J. **C77**, 225 (2017) [arXiv:1510.09010].
- [21] A. Khmelnitsky and V. Rubakov, JCAP 2 (2014) 019; N.K. Porayko and K.A. Postnov, Phys. Rev. D **90**, 062008 (2014) [arXiv:1408.4670].
- [22] A. Aoki and J. Soda, [arXiv:1608.05933].
- [23] A. Arbey, J. Lesgourgues, P. Salati, Phys.Rev. D **68**, 023511 (2003) [astro-ph/0301533]; F. Siddhartha Guzman, L. A. Urena-Lopez, Phys.Rev. D **68**, 024023 (2003) [astro-ph/0303440]; L. Amendola and B. Barbieri, Phys. Lett. B **642**, 192 (2006) [hep-ph/0509257]; A. Bernal and F. Siddhartha Guzman, Phys. Rev. D **74**, 103002 (2006) [astro-ph/0610682]; Jae-Weon Lee, J.Korean Phys.Soc. 54 (2009) 2622 [arXiv:0801.1442]; L. A. Urena-Lopez, JCAP 0901 (2009) 014 [arXiv:0806.3093]; T. Matos, J.R. Luevano, I. Quiros, L. A. Ureña-López, and J.A. Vazquez, Phys. Rev. D **80**, 123521 (2009) [arXiv:0906.0396]; T. Matos, A. Vazquez-Gonzales and J. Magana, Mon. Not. Roy. Ast. Soc. **393**, 1359 (2009) [arXiv:0806.0683]; D.J.E. Marsh and P.G. Ferreira, Phys. Rev. D **82**, 103528 (2010) [arXiv:1009.3501]; A. P. Lundgren, M. Bondarescu, R. Bondarescu, J. Balakrishna, Astrophys.J. 715, L35 (2010) [arXiv:1001.0051]; T. Harko, Phys. Rev. D **83**, 123515 (2011) [arXiv:1105.5189]; A. Cruz-Osorio, F. Siddhartha Guzman, F. D. Lora-Clavijo, JCAP 1106 (2011) 029 [arXiv:1008.0027]; V. Lora, J. Magana, A. Bernal, F.J. Sanchez-Salcedo, E.K. Grebel, JCAP 1202 (2012) 011 [arXiv:1110.2684]; A. J. Christopherson, J. Carlos Hidalgo, K. A. Malik, JCAP 1301 (2013) 002 [arXiv:1207.1870]; E.J.M. Madarassy, V.T. Toth, Comput.Phys.Comm. 184, 1339-1343 (2013) , Comput.Phys.Comm. 184, 1339-1343 (2013) [arXiv:1207.5249]; A. Surez, V.H. Robles, T. Matos, *A Review on the Scalar Field/Bose-Einstein Condensate Dark Matter Model*, [arXiv:1302.0903]; E. Castellanos, C. Escamilla-Rivera, A. Macas, D. Nez, JCAP 1411 (2014) no.11, 034 [arXiv:1310.3319]; L. Arturo Ureña-López, Phys. Rev. D **90**, 027306 (2014) [arXiv:1310.8601]; T. Harko, Phys. Rev. D **89**, 084040 (2014) [arXiv:1403.3358]; A. Diez-Tejedor, A. X. Gonzalez-Morales, S. Profumo, Phys. Rev. D **90**, 043517 (2014) [arXiv:1404.1054]; L. Visinelli, JCAP 1607 (2016)009 [arXiv:1509.05871]; J.A.R. Cembranos, A.L. Maroto, S. J. Nez Jareo, JHEP 1603, 013 (2016) [arXiv:1509.08819]; Jae-Weon Lee, Phys. Lett. B **756**, 166 (2016) [arXiv:1511.06611]; A. X. Gonzalez-Morales, D.J.E. Marsh, J. Peñarrubia, L. A. Ureña-López, [arXiv:1609.05856]; L. Arturo Ureña-López and Alma X. Gonzalez-Morales, JCAP07(2016)048 [arXiv:1511.08195].
- [24] D. J. E. Marsh, Phys.Rept. **643**, 1-79 (2016) [arXiv:1510.07633].
- [25] A. R. Liddle and A. Mazumdar, Phys. Rev. D **61**, 123507 (2000) [astro-ph/9912349].
- [26] P.G. Ferreira and M. Joyce, Phys. Rev. Lett. **79**, 4740 (1997).
- [27] B. Ratra, and P.J.E. Peebles, Phys. Rev. D **37**, 3406 (1998).
- [28] I. Zlatev, L. Wang and P.J. Steinhardt, Phys. Rev. Lett. **82** 896 (1999); P.J. Steinhardt, L. Wang, and I. Zlatev, Phys.Rev. D **59** 123504 (1999).
- [29] R. H. Brandenberger, Phys. Rev. D **32**, 501 (1985).
- [30] M. C. Johnson and M. Kamionkowski, Phys. Rev. D **78**, 063010 (2008) [arXiv:0805.1748].
- [31] E. Silverstein and A. Westphal, Phys. Rev. D **78**, 106003 (2008) [arXiv:0803.3085].
- [32] E. V. Linder, Phys. Rev. D **91**, no. 12, 123012 (2015) [arXiv:1505.00815].
- [33] K. Dimopoulos and C. Owen, [arXiv:1703.00305].
- [34] V. Sahni, M. Sami and T. Souradeep, Phys. Rev. D **65**, 023518 (2002) [gr-qc/0105121].
- [35] S. Nojiri and S. D. Odintsov, Phys.Lett. B **637**, 139 (2006) [hep-th/0603062].
- [36] S. Dutta and R. J. Scherrer, Phys. Rev. D **78**, 083512 (2008) [arXiv:0805.0763].

- [37] L. Kofman, A. D. Linde and A. A. Starobinsky, Phys. Rev. Lett. **73**, 3195 (1994) [hep-th/9405187]; Y. Shtanov, J. H. Traschen and R. H. Brandenberger, Phys. Rev. D **51**, 5438 (1995) [hep-ph/9407247].
- [38] M. Bastero-Gil, R. Cerezo and João G. Rosa, Phys. Rev. D **93**, 103531 (2016) [arXiv:1501.05539].
- [39] N. N. Bogoliubov and Y. A. Mitropolsky, *Asymptotic Methods in the Theory of Non-Linear Oscillations*, Gordon and Breach, New York (1961), 537 p.